A STUDY OF TURBULENCE CHARACTERISTICS OF SOME TURBULENT FLOWS USING EXPERIMENTAL DATA WITH APPLICATION OF QUANTIC BEHAVIOR OF TURBULENCE.

A THESIS SUBMITTED TO
THE GRADUATE SCHOOL OF NATURAL AND APPLIED SCIENCES
OF
MIDDLE EAST TECHNICAL UNIVERSITY

BY

ILGIN ÇOLAK

IN PARTIAL FULFILLMENT OF THE REQUIREMENTS
FOR
THE DEGREE OF MASTER OF SCIENCE
IN
AEROSPACE ENGINEERING

FEBRUARY 2022

Approval of the thesis:

A STUDY OF TURBULENCE CHARACTERISTICS OF SOME TURBULENT FLOWS USING EXPERIMENTAL DATA WITH APPLICATION OF QUANTIC BEHAVIOR OF TURBULENCE.

submitted by **ILGIN ÇOLAK** in partial fulfillment of the requirements for the degree of **Master of Science in Aerospace Engineering Department, Middle East Technical University** by,

Prof. Dr. Halil Kalıpçılar
Dean, Graduate School of **Natural and Applied Sciences** _____

Prof. Dr. Serkan Özgen
Head of Department, **Aerospace Engineering** _____

Assist. Prof. Dr. Mustafa Perçin
Supervisor, **Aerospace Engineering, METU** _____

Prof. Dr. Cahit Çıray
Co-supervisor, **Aerospace Engineering, METU** _____

Examining Committee Members:

Prof. Dr. Sinan Eyi
Aerospace Engineering, METU _____

Assist. Prof. Dr. Mustafa Perçin
Aerospace Engineering, METU _____

Prof. Dr. Cahit Çıray
Aerospace Engineering, METU _____

Prof. Dr. M.Metin Yavuz
Mechanical Engineering, METU _____

Prof. Dr. H.Nafiz Alemdaroğlu
Aerospace Engineering, Atılım University _____

Date: 10.02.2022

I hereby declare that all information in this document has been obtained and presented in accordance with academic rules and ethical conduct. I also declare that, as required by these rules and conduct, I have fully cited and referenced all material and results that are not original to this work.

Name, Surname: Ilgın Çolak

Signature :

ABSTRACT

A STUDY OF TURBULENCE CHARACTERISTICS OF SOME TURBULENT FLOWS USING EXPERIMENTAL DATA WITH APPLICATION OF QUANTIC BEHAVIOR OF TURBULENCE.

Çolak, Ilgın
M.S., Department of Aerospace Engineering
Supervisor: Assist. Prof. Dr. Mustafa Perçin
Co-Supervisor: Prof. Dr. Cahit Çıray

February 2022, 84 pages

Turbulence is an important phenomenon in aerospace sciences, but it still has aspects that are not fully illuminated. In order to understand the physical mechanisms of turbulence, it is crucial to consider it in terms of eddies. Eddies are the groups of fluid particles that move together and preserve a certain identity for a while, and they constitute the building blocks of turbulence. The motion of eddies in the course of their life span can be expressed as dispersive wave motion. This requires a dispersion relation, that is the frequency and the wavelength must be related by a quantity having the dimensions of velocity. The dispersion relation that is commonly used in literature is suggested by G.I Taylor based on his Frozen Turbulence hypothesis. However, it has certain limitations such that it represents only the universal equilibrium region of the spectrum to acceptable accuracy. Also, turbulence intensity must be low. Quantic Behavior of Turbulence (QBT), is suggested by Çıray[6] as an alternative and it aims to represent the physics of turbulence more accurately and in a more universal manner without the aforementioned restrictions. Moreover, it asserts that turbulence has both particle and wave-like character, which is why it is called

quantic. QBT introduces a new dispersion relation that relates wavenumber with frequency by means of group velocity, which is, at the same time fluctuating component of the instantaneous velocity. This thesis is based on QBT approach of Çıray. The aim of the study is to apply the mathematical consequences of QBT to different experimental data by utilizing a MATLAB code developed for this purpose and to analyze the results considering the physics of turbulence. Using the mathematical procedure of QBT, the code produces energy spectra on frequency out of the experimental data, and using that information obtains wavenumbers that correspond to the frequencies. In this study, two different turbulent flow data are examined. For both of them, spectra on wavenumber is obtained and comparison shows that they are compatible with the studies in the literature. Also, eddie sizes, which are obtained as wavelengths, are quite meaningful when the physical domains are considered. Thus, it is concluded that the QBT and its application in this thesis study can be very helpful to understand the physical mechanism of turbulence.

Keywords: turbulence, convective velocity, dispersion relation, quantic behaviour

ÖZ

TÜRBÜLANSIN KUANTIK DAVRANIŞI YAKLAŞIMIYLA DENEYSEL VERILER ÜZERINDEN BAZI TÜRBÜLANSLI AKIMLARIN ÖZELLIKLERINE İLIŞKIN BIR ÇALIŞMA

Çolak, Ilgın
Yüksek Lisans, Havacılık ve Uzay Mühendisliği Bölümü
Tez Yöneticisi: Dr. Öğr. Üyesi. Mustafa Perçin
Ortak Tez Yöneticisi: Prof. Dr. Cahit Çıray

Şubat 2022 , 84 sayfa

Türbülans olgusu havacılık ve uzay biliminde önemli bir yer tutmaktadır ve hala bu olgunun aydınlatılmamış yönleri bulunmaktadır. Türbülansın fiziksel mekanizmasını anlamak için onu çevrinitiler bağlamında ele almak kritik bir husustur. Bir süre boyunca birlikte hareket eden ve belirli bir kimliği koruyan akışkan parçacıkları toplulukları 'çevrinti' diye adlandırılmaktadır ve çevrintiler türbülansın yapıtaşlarını teşkil ederler. Çevrintilerin yaşam süreleri boyunca olan hareketleri saçılımlı dalga hareketi olarak tanımlanabilir. Bunun için frekansın ve dalgaboyunun iletim hızı aracılığı ile ilişkili olduğu bir saçılım ilişkisi gerkelidir. Literatürde en sık kullanılan saçılım ilişkisi , G.I Taylor tarafından kendi Donuk Türbülans hipotezi kapsamında geliştirilmiş olan ilişkidir. Fakat bu ilişki çeşitli kısıtlamalara sahiptir. Öyle ki, bu ilişki spekturumun sadece evrensel denge bölgesini yeterli derecede temsil etmektedir. Bir diğer kısıtlama ise akışın uniform ve türbülans yoğunluğunun düşük olmasının gerkeliliğidir. Bu tez çalışmasının üzerine kurulduğu Türbülansın Kuantik Davranışı (TKD) yaklaşımı ise, Taylor' un saçılım ilişkisine alternatif bir saçılım ilişkisi önerir. Çıray[6] ta-

rafından geliştirilen, bu yaklaşım, türbülans fiziğini daha doğru temsil etmeyi ve bunu yukarıda bahsedilen kısıtlamalar olmadan daha evrensel bir kapsamda yapmayı amaçlar. Ayrıca bu yaklaşım türbülansın hem dalga hem de parçacık karakterine sahip olduğunu iddia etmektedir ve bu yüzden de türbülansın davranışı kuantik' olarak adlandırılmıştır. TKD nın tanımladığı yeni saçılım ilişkisi, dalga sayısı ve frekans arasında grup hızı aracılığıyla bir ilişki kurar. Buradaki grup hızı aynı zamanda anlık hızın salınan bileşenidir. Bu tez çalışmasının amacı, geliştirilen MATLAB kodunu kullanarak farklı deneysel verilere TKD'nin matematiksel yöntemini uygulamak ve türbülans fiziğini göz önünde bulundurarak sonuçları analiz etmektir. Bahsedilen kod TKD yaklaşımının matematiksel yöntemini kullanarak deneysel verilerden frekansa bağlı enerji spektrumları oluşturur ve bu bilgilerden yola çıkarak frekanslara karşılık gelen dalga sayılarını elde eder. Bu çalışmada iki farklı türbülant akış rejimine ait deneysel veriler incelenmiştir. İki veri için de, dalga saysına bağlı spektrum elde edilmiş ve karşılaştırmalar, elde edilen spektrumun literatür ile uyum sağladığını göstermiştir. Ayrıca dalgaboyu olarak elde edilen çevrinti boyutları da akışın gerçekleştiği fiziksel ortamın boyutları göz önüne alındığında oldukça anlamlıdır. Bu sonuçlar göz önünde bulundurularak bu tez çalışmasındaki TKD ve onun uygulamalarının türbülansın fiziksel mekanizmasını anlamakta oldukça faydalı olabileceği sonucunu çıkarmak mümkündür.

Anahtar Kelimeler: türbülans, iletim hızı, saçılım ilişkisi, kuantik davranış

To Prof.Dr.Cahit Çıray,

who is truly an inspirational person with his

endless motivation for learning and teaching.

ACKNOWLEDGMENTS

First of all, I would like to thank Prof.Dr. Cahit Çıray as he provided me with the opportunity to study this topic with him. I am proud to be his student not only for his lectures that I learned a lot from but also for the enthusiasm for the science he shared with us when he teaches. I am also very glad to know him personally and thankful for all the times we have shared.

I also would like to express my thanks to Assist.Prof.Dr. Mustafa Perçin for encouraging me to study in the aerodynamics laboratory and his support on the experimental part of my study.

In addition, I would like to thank M.Tuğrul Akpolat, Fırat Kıyıcı, and Battal Gencer for sharing their experimental data and helping me to understand their experiments. Also, I would like to thank RÜZGEM for giving me the chance to gain experience in the aerodynamics laboratory. I am grateful to Anas Abdulrahim for his genuine effort to teach me the basic procedures in the aerodynamics laboratory in RUZGEM. Besides, I express my thanks to Derya Kaya, the department secretary, for making everything easier for me during the thesis preparation.

I also thank my dear friend and colleague Elif Bekoğlu who shared her experience and knowledge with me, I am happy to know her and thankful for her support.

As always, I am very grateful to have such a supportive family and I appreciate their love and patience. I especially thank my younger brother Yüce Çolak for his support.

I would like to thank my dearest, Taha Göker Gökçınar for his endless support in good and hard times. Also, I want to thank my precious friends Salih Gökmen, Merve Eşdur, İlknur Çoban, and Alperen Gündoğan for all the good times we had and we will have.

TABLE OF CONTENTS

ABSTRACT v

ÖZ vii

ACKNOWLEDGMENTS x

TABLE OF CONTENTS xi

LIST OF TABLES xiv

LIST OF FIGURES xvi

LIST OF ABBREVIATIONS xviii

CHAPTERS

1 INTRODUCTION 1

1.1 About Turbulence 1

1.1.1 Eddies 3

1.2 Taylor's Frozen Turbulence Approach 6

1.3 Literature on Taylor's Approach 7

1.4 QBT Approach 10

1.5 The Outline of the Thesis 14

2 QBT APPROACH 15

2.1 Mathematical Procedure of QBT 15

2.1.1 Obtaining Spectra in Frequency 15

2.1.2 Obtaining Spectra in Wavenumber 17
2.1.3 The Probability Density Function (PDF) 17
2.1.3.1 Properties of PDF 17
2.1.3.2 Expression of the PDF Used in QBT 18
2.1.3.3 Finding *P(1)* 19
2.1.3.4 Finding *A* 21
2.1.3.5 Finding μ^{κ} 22
2.1.4 Discrete Form of Working Equations 23
2.1.5 Initiation of Calculation of Working Equations 24
2.1.5.1 Expression of x_1 24
2.1.5.2 Expression of $k(f)$ 25
3 METHOD 27
3.1 Introduction 27
3.2 First Part: Fourier Transforms 27
3.2.1 inputs 27
3.2.2 $'fft'$ command 27
3.2.3 Energy Densities 28
3.2.4 Integration and Nondimensionalization of Energy Densities . . 29
3.3 Second Part: The PDF 29
3.3.1 Inputs 29
3.3.2 Finding μ^2 and n 29
3.3.3 Finding PDF 30
3.3.4 Finding k 32

3.3.5 Verification of the code 32

4 RESULTS 33

4.1 On Experimental Results 33

4.2 Micro Vortex Generator Experiment 33

4.2.1 Introduction 33

4.2.2 Setup and Method 34

4.2.3 Analysis 35

4.2.4 Results 36

4.3 The Experiment of Unconfined and Non swirling Jet 43

4.3.1 Setup and Method 43

4.3.2 PDFs and Histograms 47

4.3.2.1 Spectral Study 52

5 CONCLUSIONS 57

REFERENCES 61

APPENDICES

LIST OF TABLES

TABLES

Table 2.1 Transformations for equations 2.19and 2.20 20

Table 2.2 Transformation for equations 2.20and 2.34 22

Table 4.1 Comparison of undisturbed and MVG cases based on largest wavelength, turbulence intensity and mean velocity 42

Table 4.2 Some characteristics of the flow at 0.3D location 54

Table 4.3 Some characteristics of the flow at 0.5D location 54

Table 4.4 Some characteristics of the flow at 1D location 55

Table .1 Results of Undisturbed case at 14mm 63

Table .2 Results of Undisturbed case at 34mm 64

Table .3 Results of Undisturbed case at 54mm 65

Table .4 Results of Undisturbed case at 74mm 66

Table .5 Results of MVG case at 14mm 67

Table .6 Results of MVG case at 34mm 68

Table .7 Results of MVG case at 54mm 69

Table .8 Results of MVG case at 74mm 70

Table .9 Results for 0.3D location and at 0 mm 71

Table .10 Results for 0.3D location and at 6 mm 72

Table .11 Results for 0.3D location and at 10 mm 73

Table .12 Results for 0.3D location and at 14 mm 74

Table .13 Results for 0.5D location and at 0mm 75

Table .14 Results for 0.5D location and at 6 mm 76

Table .15 Results for 0.5D location and at 10 mm 77

Table .16 Results for 0.5D location and at 14 mm 78

Table .17 Results for 0.5D location and at 18 mm 79

Table .18 Results for 1D location and at 0mm 80

Table .19 Results for 1D location and at 6mm 81

Table .20 Results for 1D location and at 10 mm 82

Table .21 Results for 1D location and at 14 mm 83

Table .22 Results for 1D location and at 18 mm 84

LIST OF FIGURES

FIGURES

Figure 1.1 Taylor's 1-D spectrum 3

Figure 1.2 3D Energy Spectrum and Regions[7] 4

Figure 1.3 Discrete and Wave-like Character of Turbulence[5] 12

Figure 1.4 The representation of $P(x)$ and $P(x)u^2$ terms reproduced from LHS of Figure 6 in [5] 13

Figure 4.1 METUWIND/RÜZGEM C3 Medium Scale Suction Type Wind Tunnel (adapted from[2]) 34

Figure 4.2 Dimensions and Geometry of MVG (adapted from [2]) 34

Figure 4.3 Placement of MVG (adapted from [2]) 34

Figure 4.4 Velocity profiles for the Undisturbed case(a) and for the MVG case(b) 36

Figure 4.5 PDFs and Histograms for the Undisturbed Case at 14mm(a), 34mm(b), 54mm(c), 74mm(d) 37

Figure 4.6 PDFs and Histograms for the MVG Case at 14mm(a), 34mm(b), 54mm(c), 74mm(d) 38

Figure 4.7 PDFs for chosen points for Undisturbed Case(a) and for the MVG Case(b) 39

Figure 4.8 Spectra based on Wave Number in Logarithmic Scale for Both Cases 40

Figure 4.9 Spectra based on Frequency for Both Cases 41

Figure 4.10 Schematic of the Non-swirling and Unconfined Jet Experiment Setup(adapted from [16]) 44

Figure 4.11 Measurement points for the Non-swirling and Unconfined Jet Experiment 44

Figure 4.12 Symmetrical Velocity Profiles for the Non-swirling and Unconfined Jet Experiment 45

Figure 4.13 One-sided Velocity Profiles for the Non-swirling and Unconfined Jet Experiment 45

Figure 4.14 PDFs and Histograms for 0.3D Location at 0mm(a), 6mm(b), 10mm(c), 14mm(d). 47

Figure 4.15 PDFs and Histograms for 0.5D Location at 0mm(a), 6mm(b), 10mm(c), 14mm(d), 18mm(e). 49

Figure 4.16 PDFs and Histograms for 1D Location at 0mm(a), 6mm(b), 10mm(c), 14mm(d), 18mm(e). 50

Figure 4.17 PDFs for 0.3D location(a), 0.5D location(b), 1D location(c) . . . 51

Figure 4.18 Spectra based on frequency for 0.3D location(a), 0.5D location(b), 1D location(C) 52

Figure 4.19 Spectra based on wavenumber for 0.3D location(a), 0.5Dlocation(b), 1D location(c) 53

LIST OF ABBREVIATIONS

ABBREVIATIONS

BL	Boundary Layer
DFT	Discrete Fourier Transform
DNS	Direct Numerical Simulation
FFT	Fast Fourier Transform
HWA	Hot Wire Anemometry
LES	Large Eddie Simulation
LHS	Left-hand-side
MVG	Micro Vortex Generator
NS	Navier-Stokes
PDF	Probability Density Function
PIV	Particle Image Velocimetry
QBT	Quantic Behavior of Turbulence
RANS	Raynolds Averaged Navier-Stokes
RHS	Right-hand-side
1-D	One Dimensional
3-D	Three Dimensional

SYMBOLS

ROMAN SYMBOLS

$a(\eta)$	Fourier coefficient of cosine term(real part) in continuous form,[m]
a_η	Fourier coefficient of cosine term(real part) in discrete form, [m/s]

$b(\eta)$	Fourier coefficient of sine term(imaginary part) in continuous form,[m]
b_η	Fourier coefficient of sine term(imaginary part) in discrete form, [m/s]
c	Phase velocity, [m/s]
f	Frequency,[Hz]
k	Wavenumber,[m^-1]
t	Time,[s]
u	Instantaneous velocity fluctuation in x direction,[m/s]
u'	Root mean square of instantaneous velocity fluctuation in x direction,[m/s]
x	Non-dimensional instantaneous velocity fluctuation in x direction[-]
y	Non-dimensional instantaneous velocity in x direction[-]
A	Constant property of PDF,[-]
B	Determined number by QBT for each data[-]
D	Diameter,[mm]
$E(k)$	Energy density per unit wavenumber,[m^3/s^2]
G	Any property of an eddy, [-]
$G(f)$	Normalized frequency-dependent energy spectrum function,[s]
I_{act}	Actual turbulence intensity found from experimental data,[-]
I_{calc}	Calculated turbulence intensity by QBT,[-]
L	Integral scale,[m]
N	The number of discrete data,[-]
$P(x)$	Probability density function(PDF) in terms of x,[-]
$P(y)$	Probability density function(PDF) in terms of y,[-]
$P(1)$	Constant property of PDF,[-]
$P_L(x)$	LHS of PDF in terms of x,[-]

$P_R(X)$	RHS of PDF in terms of x,[-]
SR	Sampling Rate,[Hz]
Q_E	Correlation function,[m^2/s^2]
T	Period,[s]
U	Instantaneous velocity in x direction, [m/s]
$\overline{U}$	Mean velocity in x direction, [m/s]
U_c	Convective velocity, [m/s]

GREEK SYMBOLS

η	Frequency, [Hz]
μ^κ	Normalized κ^{th} moment, [-]
μ^2_{act}	Normalized actual 2^{nd} order moment found from experimental data,[-]
μ^2_{act}	Normalized calculated 2^{nd} order moment by QBT,[-]
ν	Kinematic viscosity, [m^2/s]
ξ	Any variable, [-]
ω	Circular frequency, [rad/s]

CHAPTER 1

INTRODUCTION

1.1 About Turbulence

Turbulence is one of the most intriguing problems in aerospace sciences. However, turbulence is a flow regime that is essentially unsteady, that is, fluctuations in quantities are always functions of time. Also, one of the main characteristics of turbulence is randomness. This implies that quantities are random functions of time and space coordinates. Hence studying such a flow regime and building mathematical relations to describe the problem of turbulence is one of the biggest challenges. The mathematical definition of turbulence is studied either with a statistical approach or a spectral approach.

As all quantities in turbulent flow are random functions of time, each quantity has an instantaneous value at a certain time t. Reynolds[19] defines those instantaneous quantities as composed of two parts: one is the mean value, which is the mean of that quantity for a chosen time interval, and the other is the fluctuating part [7].This definition is known as 'Reynolds Splitting ' and can be represented as :

$$Q = \overline{Q} + q \tag{1.1}$$

Where, Q represents any quantity, such as a velocity component, and $\overline{Q}$ represents the mean of that quantity for a certain time and q represents fluctuations. One of the main characteristics of turbulence is that the mean quantities are deterministic functions of space and time coordinates. while fluctuating quantities are still random functions of time. However, this does not mean that ignoring the fluctuating quantities will solve the problems. In order to define the problem of turbulence mathematically, we need governing equations and boundary conditions. Here, the governing

equations are continuity equation and Navier Stokes equations if the fluid is incompressible. When Navier Stokes equations are written for the turbulent quantities in the form of Reynolds splitting, i.e as in equation1.1, we obtain Reynolds Averaged Navier Stokes (RANS) equations. However, RANS equations include an additional term when compared to NS Equations for laminar flow (with no fluctuations). This additional term is known as Reynolds stress and defined as $-\rho\overline{u_i u_j}_{,j}$ and it represents the momentum transported from the unit area of the flow. This shows that fluctuating quantities have a main role to define turbulence and must be considered in mathematical definitions of turbulence. Reynolds stress term can be defined as a symmetrical tensor, which means six additional correlations are embedded inside the NS equations for turbulent flow[7]. To solve RANS equations, which include Reynolds stress terms, RANS equations can be subtracted from the NS equations but this procedure only brings higher-order correlation terms, which in turn, increases the number of unknowns. This situation is known as the 'closure problem' of turbulence. It implies that when the statistical methods are used, numbers of equations and unknowns cannot be equated. To deal with this struggle, some turbulence models based on differential equations have been developed.

The Spectral approach, on the other hand, considers fluctuations as a superposition of sinusoidal waves. This leads to a mathematical representation of fluctuating quantities as Fourier integrals. In the spectral approach, each frequency range contributes to the total kinetic energy by some amount. This is represented by a spectrum. To explain that from the mathematical point of view, u_1 can be considered as the component of velocity fluctuations in the direction of 1, at a fixed point in a flow field. Then, u_1^2 will represent the kinetic energy of turbulent flow at this point and in this direction. Of course, this value can be averaged over a time interval[14]. On the other hand, the same energy can be represented as a sum of contributions of different frequencies. These two perspectives can be unified with an equation:

$$\overline{u}^2 = \int_0^\infty E(n)\, dn \ , \tag{1.2}$$

Here *E(n)* is the spectrum function where n is the frequency. *E(n)* also represents the kinetic energy density of fluctuations of each frequency and the integral simply means the summation of contributions of each dn interval of frequency to the kinetic energy of turbulence. Further, representing velocity fluctuations as sinusoidal waves

by means of Fourier integrals, equation 1.2 can be written again as:

$$\overline{u}^2 = \pi^2 \int_0^\infty \frac{a(n)^2 + b(n)^2}{T}\, dn = \int_0^\infty E(n)\, dn\ , \tag{1.3}$$

where T is the period and $a(n)$ and $b(n)$represents the amplitudes of the sinusodial waves. *E(n)* is known as Taylor's 1-D energy spectrum and it is schematized in the below figure.

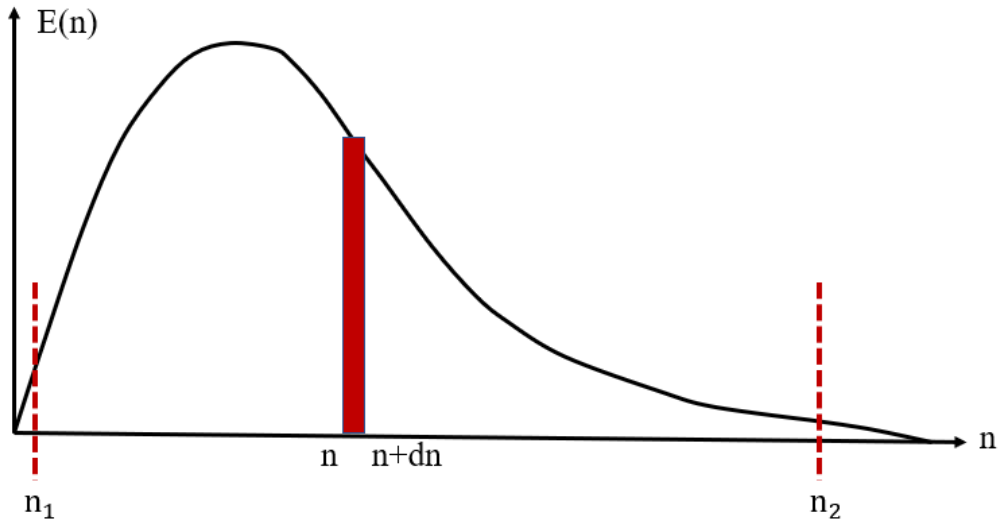


Figure 1.1: Taylor's 1-D spectrum

[7]

From the figure 1.1, it can be understood that by taking the integral, the contribution of any frequency interval between$n$ and$n + dn$ to the kinetic energy of turbulence can be found. Here, frequency values n_1 and n_2 are cut-off values for low pass and high pass filters, respectively. By filtering frequency values that are below n_1 and above n_2, the contribution of electronic noise is eliminated.

1.1.1 Eddies

After summarizing statistical and spectral approaches, it is worthwhile to mention eddies. Eddies can be considered as the building blocks of turbulence. They consist of fluid particles that move together and preserve a certain character for a while.This character may be momentum, vorticity, or something else. As the building blocks of turbulence, their formations,life spans, motions, sizes, and velocities are random

functions of space and time. Velocities of eddies can be studied from a dispersive wave point of view and their wavelength corresponds to the size of the eddies[**?**]. The sizes of the eddies are different; they can be in the order of mm or smaller, or they can be as large as the dimensions of the boundaries in which the flow takes place. For example, for a pipe flow, the largest eddie size can be equal to the diameter of the pipe. However, it is important to note that eddie sizes larger than the physical dimensions of the flow field are not reasonable [17]. Thus, the largest eddie size is a parameter that should be checked when carrying out calculations, if physically meaningful results are desired. Also, eddies do not preserve their sizes throughout their life span; they continuously divide and form smaller eddies and also transfer their energies to new eddies. This is called energy cascading and in the course of this process they also lose some of their energy due to viscosity.

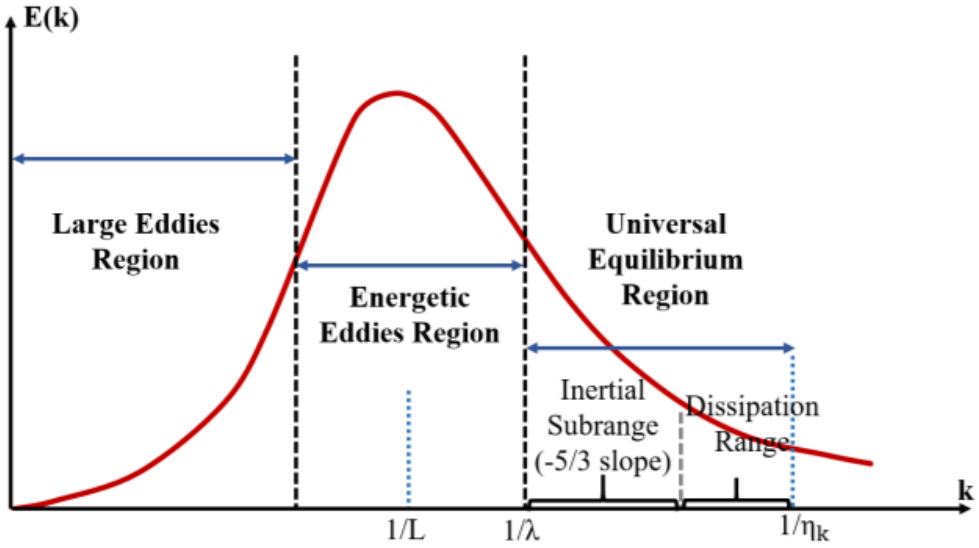


Figure 1.2: 3D Energy Spectrum and Regions[7]

In the figure 1.2, 3D energy spectrum based on wavenumber, k is demonstrated. This spectrum is obtained using three-point double velocity correlations. Wavelengths represent eddie sizes and thus, small wave numbers correspond to big eddies and large wave numbers correspond to smaller eddies. The first region is the *Large Eddies Region*. Large eddies are formed when the velocity gradients are significant and viscosity is relatively less effective in the formation of these eddies. For example, near the rigid boundaries largest eddies may form. In other words, large eddies represent

the boundary effects. Also, this region includes 20 percent of the total kinetic energy. Hence, the role of the large eddies in understanding turbulence cannot be ignored. The second region is known as the *Energetic Eddies Region*. The eddies in this region are smaller and energy loss per eddie is smaller than in the first region. This leads to a higher energy density per wavelength. The third region is called *Universal Equilibrium Region*.In this region, eddies do not lose a significant amount of their energy, and they transfer their energy to smaller eddies faster than they lose energy. Therefore, it can be inferred that this region is an equilibrium state. Eddies in this region are formed by the division of larger eddies which were affected by the boundary conditions. However, these smaller eddies are independent of the boundary conditions and effect of velocity gradients. Therefore, this region has a universal character. Besides, this region shows an isotropic character, and different turbulence models can represent this region well enough. However, unlike Universal Equilibrium Region, Large Eddies Region bears the effect of the boundaries, hence, for each different boundary condition, some adaptations in the solutions, such as changing correction constants are needed[7]. Large Eddie Simulation (LES) is a method for modeling the boundary conditions of the flow field, therefore a method for modeling turbulence including the effect of large eddies and considering their energy contribution. LES is used for the flows around blunt bodies, wedges, etc., and for analyzing the flow in separation. However, while it is good for modeling large eddies region, LES does not perform well enough for the regions with larger wave numbers[7].

For turbulence is a random phenomenon, relations between quantities in a turbulent flow can be mathematically represented by correlations. Eddies are defined as the fluid particles that behave similarly or move together for a while, thus, correlations are used for the determination of sizes and life spans of the eddies. For example, velocity correlations are used to have an idea of the size of the eddies. Similarly, correlations based on time provide information about the life spans of the eddies. However, a relation between the spatial and temporal quantities is required[7].

1.2 Taylor's Frozen Turbulence Approach

To establish a relation between the spatial and temporal quantities of turbulent flow, G.I.Taylor suggested[12]:

$$dr = \overline{U}dt \tag{1.4}$$

where $\overline{U}$ represents the mean flow velocity which is also the convective velocity. Convective velocity is the velocity that the turbulence quantities are transported from one location to another one. Equation1.4 implies that any quantity of turbulence at a location $\xi - \Delta\xi$ is transported without change with the velocity $\overline{U}$ within the interval Δt to the location ξ. In other words, in turbulent flow field which is frozen at $\xi - \Delta\xi$ and at t-Δt, a quantity G a will be only a function of space coordinates. Therefore, at ξ, the change of G with time is due to the transportation of frozen turbulence with the velocity $\overline{U_1}$. That is, quantity G depends on time not directly, but via $\overline{U_1}$[7]. This can be expressed mathematically by the following equation:

$$G(t)|_\xi = G(\xi - \overline{U_1}\Delta t) = G(\eta) \tag{1.5}$$

Also,

$$\lim_{\Delta t \to 0} \frac{\Delta G}{\Delta t}\bigg|_\xi = \lim_{\Delta t \to 0} \frac{\Delta G}{\Delta \eta}\frac{\delta \eta}{\delta t} \tag{1.6}$$

where,

$$\lim_{\Delta t \to 0} \frac{\Delta G}{\Delta \eta} = \frac{\delta G}{\delta \xi}\bigg|_\xi \tag{1.7}$$

and

$$\frac{\delta \eta}{\delta t} = -\overline{U} \tag{1.8}$$

Therefore,

$$\frac{\delta G}{\delta t} = -\overline{U}\frac{\delta}{G}\delta\xi \tag{1.9}$$

This can also be expressed as:

$$\frac{\delta G}{\delta t} + \overline{U}\frac{\delta G}{\delta \xi} = 0 \tag{1.10}$$

or as:

$$\frac{DG}{Dt} = 0 \tag{1.11}$$

Equation1.11 is a result of frozen turbulence and it shows that quantity G is transported to the point ξ without a change with respect to time.

This conclusion is based on the condition that mean velocity $\overline{U}$ is much greater than the root mean square of the fluctuation velocities, $\sqrt{\overline{(u_1)^2}}$.

Taylor's Frozen Turbulence approach is physically meaningful if the turbulence is homogeneous and isotropic because, for this kind of turbulence, correlations are the same everywhere and in every direction[7]. This is the situation for the Universal Equilibrium Region in the figure1.2. For this region, Taylor's Frozen Turbulence approach gives accurate results.

If the problem is examined in terms of eddies, as their velocities in the course of their life spans have dispersive-wave characteristics, a relation between the wavelength and frequency is also needed[5]. The consequence of the frozen turbulence is:

$$k = \frac{f}{\overline{U}} \tag{1.12}$$

where k is wavenumber and f is frequency of the fluctuating part u of the instantaneous velocity, and is the mean velocity. Similar to equation 1.10, this equation also implies that any fluctuating quantity within an eddie, will be transported with the mean velocity $\overline{U}$, without any loss. However, employing this relation leads to eddie sizes larger than the intrinsic dimensions of the domain in which flow takes place. As mentioned before, this is not a physically reasonable result. Thus, this relation is not helpful for the small wavenumbers region representing larger eddies. Besides, Taylor himself accepts that this approach is limited to regions with low turbulence intensity. Therefore, the use of Taylor's approach is restricted to Universal Equilibrium Region for which eddie sizes do not depend on boundary conditions and the local structure of turbulence[7].

1.3 Literature on Taylor's Approach

In his paper in 1953, C.C Lin discusses Taylor's hypothesis in the case of shear flow and aims to find out to which extent the hypothesis is valid. He examined the order of magnitude of the various acceleration terms in the equations of motion, especially the acceleration due to the pressure gradient. Considering inertial acceleration terms are dominant for large Reynolds numbers, pressure acceleration terms can be ignored

compared to them. If equations of motion are taken into account,

$$\frac{\delta u_i}{\delta t} + U\frac{\delta u_i}{\delta x} + u_i\frac{\delta u_i}{\delta x_j} = -\frac{1}{\rho}\frac{\delta p}{\delta x_i} + \nu\Delta u_i \tag{1.13}$$

first two terms are considerably larger than the rest according to Taylor's hypothesis. However, to ignore the pressure terms, Lin shows the following conditions must be satisfied:

$$\frac{\delta U}{\delta y} = 0 \tag{1.14}$$

and

$$\frac{\delta^2 U}{\delta y^2} = 0 \tag{1.15}$$

That is, pressure terms can be ignored only when the flow is uniform. Therefore, Lin concludes that Taylor's hypothesis cannot be extended to the shear flow.

Also, in the study of Goldschmidt et al. convective velocity is defined as the division of the distance between two measurement points to the time to reach maximum correlations[13]:

$$U_c = x_s/_m \tag{1.16}$$

According to Taylor's approach U_c defined in the above relation must be equal to $\overline{U}$, the local mean velocity. Goldschmidt et al.(1981) used a jet experiment data to observe the frequency ranges for which $U_c = \overline{U}$. As a result of this study, it is found that the ratio $U_c/\overline{U} > 1$ for $y/b > 0.8$ where y/b is defined as the dimensionless ratio of lateral coordinate and the half-width of the jet. However, Taylor's hypothesis is valid for the $y/b <= 0.8$ in the self-similar region of the jet. Also, as a result of the frequency analysis, it is found that the large eddies move slower than the mean flow while the smaller eddies move faster[13]. Besides, many other results from various researchers are tabulated in the study of Goldschmidt et al.[13]. From the table, it can be concluded that the ratio of convective velocity and local mean velocity depends on the flow field and region, region of the test, and the definition of convective velocity chosen for the analysis. For example, Fisher and Davies(1964) used an alternative definition for convective velocity. To do that, they plotted various cross-correlation curves each of which represents a different probe separation. The definition of the convection velocity is based on a time delay,$_e$ at which the envelope of all the cross-correlation curves intersects the curve for a certain probe separation[10]. Thus the

convective velocity is:

$$U_c = x_s/_e \tag{1.17}$$

where,$_e$ is the time delay.

They perform the experiments mainly for a mixing region of a jet, and results have shown that in the case of shear and high turbulence intensity, Taylor's Frozen Turbulence approach does not perform well. They concluded that the differences between the mean velocity and convection velocity are because of the skewness of the probability distribution of the velocity fluctuations[10].

Lee et al.(1992) introduced a method for producing inflow turbulence fluctuations for spatially developing turbulence and used it for a DNS of spatially evolving isotropic turbulence. From their results, they conclude that Taylor's hypothesis is successful enough in the case of solenoidal motion such as vorticity, however, it fails for purely compressible motion such as dilatation[18].

It can be observed that most of the effort is focused on defining convection velocities that can be used instead of the mean velocity in Taylor's hypothesis. However, recent studies concern more about spectral approaches rather than the correlation-based techniques[15]

For Example, del Alamo and Jimenez(2009) introduce a new method that depends on spectral information in only one direction(space or time) and on time derivatives for the other directions to estimate the convective velocities[4]. The obtained convection velocity is defined as $c = \omega_0/k_x$ where ω_0 is the location of the center of gravity of the spectrum for a constant wavenumber. As a result of applying their method to numerical simulation data, they suggest that the method can be used for correcting the errors that are spring from Taylor's approach which uses a convective velocity that does not depend on eddie size. They also add that Taylor's approach leads to aliasing the large scales into shorter ones near the boundaries as they move faster than the local mean velocity. Besides, Taylor's approach causes deformation in the spectrum, especially for higher for higher Reynolds numbers[3].

Tardu and Vezin(2015) performed a DNS study for low Reynolds number turbulent channel flow to observe the limitations of Taylor's approach. They found out that

the frozen turbulence approach fails in the viscous sublayer and provides a rough approximation for the buffer layer, while it represents the upper regions well[11]. Also, they conclude that this departure from the Taylor's approach in the buffer and viscous sublayers results from the production and pressure gradient terms[21].

Geng et al. performed DNS analysis for turbulent channel flow both with a low and a high Reynolds number. They derive an expression for optimal convection velocities using space and time derivatives of instantaneous fluctuating velocities. Their results also support the result obtained from del Alamo and Jimenez[11].

De Kat and Ganapathisubramani(2015) intorduced a cross-spectral approach using phase differences between two points to obtain the wavenumber-frequency plane from which spatial spectrum can be formed. They used a turbulent boundary layer data acquired by PIV technique. It is a data-driven method and can be put into practice for different shear flows without using Taylor's hypothesis. Comparing the results of their method and the ones obtained using Taylor's approach, they found that while Taylor's approach can represent larger wavenumber regions of the spectrum, there are significant differences for small wavenumber ranges[15].

In the light of these studies in literature, it becomes certain that Taylor's approach has limitations. Conditions under which it is valid should be known to use its implementations in the analysis of experimental data. Also, it can be inferred that new approaches are required to solve the physics of turbulence.

1.4 QBT Approach

In the preceding sections, the limitation of Taylor's Frozen Turbulence approach is explained in detail. The conditions under which Taylor's hypothesis is valid can be summarized as:

- Flow must be uniform
- Turbulence intensity must be low
- Reynolds number should be high

- The wavelength must be much less than the boundary layer thickness

Also, some suggestions to find convection velocities that work better for the cases for which Taylor's hypothesis fails are summarized. In addition, some recent studies that make use of new methods and develop new approaches are discussed.

This section aims to explicate the Quantic Behaviour of Turbulence Approach developed by Çıray [**?**] with regard to its main idea and in connection with the historical development of the problem. The mathematical details, except the main equations, will be handled in Chapter 2.

QBT aims to find a universal dispersion relation that applies to all regions of the spectrum. Unlike Taylor's hypothesis, it is aimed to represent the Large Eddies Region accurately as well as the other regions. And unlike Large Eddie Simulations, it aims to cover the regions with smaller eddies with a high level of precision.

The motivation of QBT is understanding the physical mechanism of turbulence truly and representing it mathematically without being estranged from its physical essence. Therefore, unlike the models which tries to certain solutions for specific problems with certain boundary conditions, it tries to grasp the physical mechanism and thus find mathematical definitions which is valid under any boundary condition.

In QBT, a new dispersion relation is suggested:

$$u = \frac{d\omega}{dk}, \tag{1.18}$$

where ω and k are defined as before, and u here is fluctuation velocity where in the Taylor's approach convective velocity is taken as $\overline{U}$. The Equation 1.18 provides a basis for QBT. As mentioned before, eddies are particles that move as a group and their motion can be represented as dispersive wave motion. Thus, it is convenient to say that the frequency and wavenumber of an eddie are related to each other by group velocity. Group velocity can be defined as the convection velocity of the energy and translation velocity of the mass. It means that eddies move with u and they transform their energy with u. As a result, the main assertion of QBT Approach is that the fluctuation velocity is in fact, the group velocity of the wave[5]. In other words, the

fluctuating velocity is the energy transport velocity that carries the turbulence energy by means of the ”discrete material packages”, that is the eddies of finite lifespan[9]. The approach named ’Quantic Behavior of Turbulence’ due to the simultaneous wave-like and discrete behavior of turbulence. Figure1.3 depicts that dual character of turbulence.

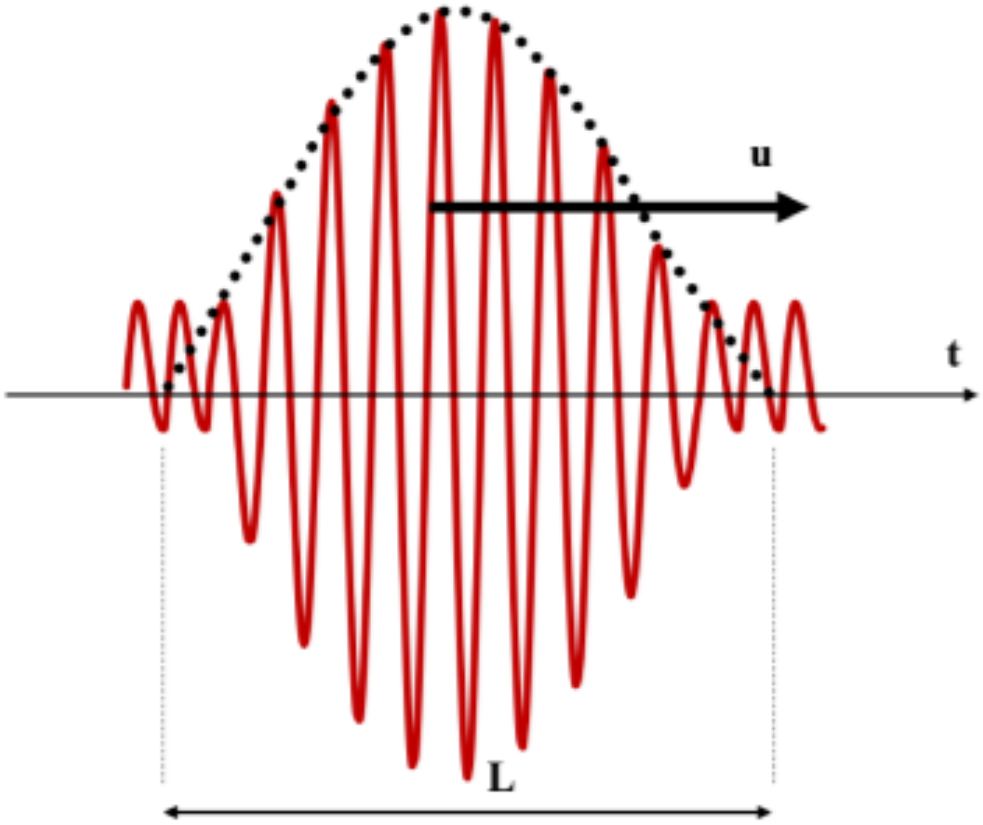


Figure 1.3: Discrete and Wave-like Character of Turbulence[5]

Second main equation of the QBT is:

$$\int_{-\infty}^{\infty} P(x)u^2\,dx = u'^2 \int_{0}^{\infty} G(f)\,df, \tag{1.19}$$

Here, in the left-hand side of the equation,x is non-dimensional instantaneous fluctuation velocity, $P(x)$ is PDF, representing the probabilities of the fluctuations.

x can be defined as:

$$x = \frac{u}{u'}$$

The term $P(x)u^2$, therefore, represents the energy contributions of the fluctuations. The terms $P(x)$ and $P(x)u^2$ are demonstrated in the figure 1.4.

On the right-hand side,f is frequency, $G(f)$ is the spectrum function and u' is the root-mean-square (rms) of instantaneous velocity fluctuations. The kinetic energy of the fluctuations can be represented as the average of the square of the fluctuation velocities, i.e, $\overline{u^2}$. Then,

$$u'^2 = \overline{u^2} = u'^2 \int_0^\infty G(f)df, \tag{1.20}$$

And,

$$\int_0^\infty G(f)df = 1. \tag{1.20}$$

Equation1.20 is a relation that contains the true characteristics of the turbulence at any point of interest. Thus, the calculations based on this relation correspond to the true physics of the turbulence.[5]

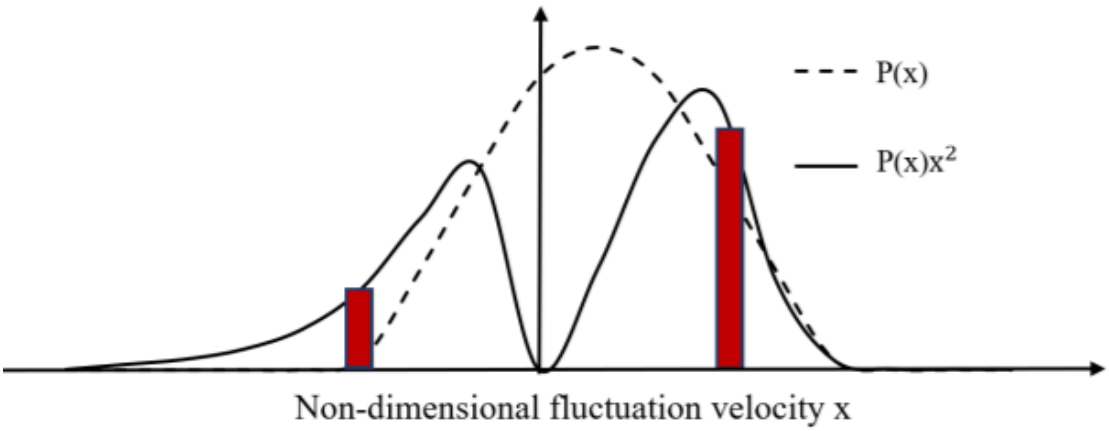


Figure 1.4: The representation of $P(x)$ and $P(x)u^2$ terms reproduced from LHS of Figure 6 in [5]

In this section, equations 1.18 and 1.19 are defined as the main equations of QBT.

The remaining mathematical procedure is discussed in Chapter 2.

1.5 The Outline of the Thesis

Until now, the main characteristics of turbulent flow are mentioned and approaches towards understanding turbulence are discussed. Also, the main issues of turbulence and the solutions suggested regarding those problems are expressed. Following that, the main idea of the QBT approach, which this thesis is based on, is defined. In the subsequent chapters, the following points will be discussed:

- Mathematical definition of QBT in more detail(Chapter 2, QBT Approach)
- The computer code based on QBT approach for analyzing experimental data (Chapter 3, Method)
- the explanation of two different experiments conducted and the results of analysis experimental data (Chapter 4, Results)
- Final conclusions regarding the obtained results and QBT approach (Chapter 5, Conclusions)

CHAPTER 2

QBT APPROACH

2.1 Mathematical Procedure of QBT

In the previous chapter, equations 1.18 and 1.19 are defined as the main equations of QBT. In this section, how this PDF is obtained will be explained in detail. Also, how the spectrum function is obtained using the experimental data and utilizing Fourier Integrals will be discussed.

2.1.1 Obtaining Spectra in Frequency

As mentioned in the previous chapter, the spectral approach considers fluctuating velocities as the superposition of an infinite number of sinusoidal wave functions, each of which has a frequency. In addition, all frequency interval contributes to the total kinetic energy of turbulence by some amount. Hence,

$$u(t) = 2\pi \int_0^\infty \left[a(\eta)cos(2\pi\eta t) + b(\eta)sin(2\pi\eta t)\right] d\eta \tag{2.0}$$

where t is time and η is the frequency.Also, $a(\eta)$ and $b(\eta)$ are called as Fourier coefficients and they are given as :

$$a(\eta) = \frac{1}{\pi} \int_{-\infty}^{\infty} u(t)cos(2\pi\eta t)\, dt\ , \tag{2.1a}$$

$$b(\eta) = \frac{1}{\pi} \int_{-\infty}^{\infty} u(t)sin(2\pi\eta t)\, dt \tag{2.1b}$$

However,the condition of validity for Fourier integral given in 2.0 is :

$$\int_{-\infty}^{\infty} |u(t)| = finite. \tag{2.2}$$

Considering a time interval 2T and assuming that outside of this interval, the integral is zero,that is $u = 0$ outside of the boundaries of the integral, Fourier transformations can be written as:

$$a(\eta) = \frac{1}{\pi} \int_{-T}^{T} u(t) cos(2\pi\eta t) dt \tag{2.3a}$$

$$b(\eta) = \frac{1}{\pi} \int_{-T}^{T} u(t) sin(2\pi\eta t) dt \tag{2.3b}$$

The experimental data used in this study consists of instantaneous velocity measurements for different points in the flow. The continuous data coming from the flow is sampled using data acquisition systems and analog to digital converters. Hence, to find Fourier coefficients, there is discrete data of $u(t)$, instead of a continuous function. The calculation of Fourier coefficients is implemented by a MATLAB code which is the subject of the third Chapter. Firstly, the coefficients are obtained by using directly the discrete form of the given equations, that is, Direct Fourier Transform(DFT). However, with this method, results are obtained approximately in 36 hours for each measurement point with 600.000 velocity data. Thus, Fast Fourier Transform(FFT) is employed as a second method. This is a special algorithm that reduces the number of operations for Fourier transform and thus, it is more efficient timewise. With FFT, calculation time is reduced to less than a second per measurement point. Also, results coming from two methods are compared and it is found that they give almost the same results. Thus, FFT is used in this study as it provides results faster without compromising accuracy. To make use of that method, the 'fft' command on Matlab is used.

After finding Fourier coefficients $a(\eta)$ and $b(\eta)$, the energy contributions can also be represented in the form of Fourier integrals according to 1.3. Equation 1.3 is obtained from the correlation function given by Hinze [14]:

$$Q_E(t) = \frac{4\pi^2}{2T + t} \int_0^{\infty} \frac{a^2(\eta) + b^2(\eta)}{2} cos(2\pi\eta t) d\eta \ , \tag{2.4}$$

and choosing t as zero,

$$\overline{u^2(0)} = \pi^2 \int_0^{\infty} \frac{a^2(\eta) + b^2(\eta)}{T} d\eta \ . \tag{2.5}$$

2.1.2 Obtaining Spectra in Wavenumber

With the help of equation 1.3, we can estimate the contribution of each frequency interval to the total kinetic energy of turbulence. Considering the second main equation of QBT given as 1.19, the right-hand side of the equation is now known. To have the spectra in the wavenumber domain, we should proceed to the left-hand side of the equation, that is, the PDF.

2.1.3 The Probability Density Function (PDF)

With the help of a PDF, knowledge of the probability distribution of any data can be obtained. Within the scope of this study, PDF is used to find out the probability distribution of velocity fluctuations of turbulent flows. In this section, firstly some general properties of PDF are defined for clarity. Then, the characteristics of the special PDF developed by Çıray[6] is explained. After that, how the PDF is used to acquire the information of wavenumbers is explained.

2.1.3.1 Properties of PDF

Before moving into the properties of PDF, it is convenient to define some characteristics :

$$U = \overline{U} + u = \overline{U}\left(1 + \frac{u}{u'}\frac{u'}{\overline{U}}\right) = \overline{U}(1 + xI) = \overline{U}y \tag{2.6}$$

$$x = \frac{u}{u'} \tag{2.7}$$

$$y = 1 + xI = \frac{U}{\overline{U}} \tag{2.8}$$

$$I = \frac{u'}{\overline{U}} \tag{2.9}$$

Here in the above equations, x is the dimensionless velocity fluctuation which is defined as the division of fluctuating component of the instantaneous velocity to the root mean square of the fluctuation velocities. Also, I is the turbulence intensity, that is the root mean square of the fluctuations divided by the mean velocity of the flow.

Using those definitions, some properties of PDF are defined as follows:

$$\int_{-\infty}^{\infty} P(y)\,dy = 1\ , \qquad (2.10a) \qquad \int_{-\infty}^{\infty} P(y)U\,dy = \overline{U}\ , \qquad (2.10c)$$

$$\int_{-\infty}^{\infty} P(x)\,dx = \frac{1}{I}\ , \qquad (2.10b) \qquad \int_{-\infty}^{\infty} P(y)y\,dy = 1\ . \qquad (2.10d)$$

Also the moment of the PDF is :

$$\mu^{\kappa} = \frac{1}{\overline{U}^{\kappa}} \int_{-\infty}^{\infty} P(y)U^{\kappa}dy \qquad (2.11)$$

where μ^{κ} is the moment of degree κ of U. Using equation 2.10b and 2.10d, we can get:

$$\int_{-\infty}^{\infty} P(y)U\,dy = \int_{-\infty}^{\infty} P(y)(\overline{U}+u)\,dy = \overline{U}\int_{-\infty}^{\infty} P(y)\,dy + \int_{-\infty}^{\infty} P(y)u\,dy = \overline{U}\ .$$

And therefore,

$$\int_{-\infty}^{\infty} P(y)udy = 0; \qquad (2.12)$$

Also,

$$\int_{-\infty}^{\infty} P(y)U^2\,dy = \int_{-\infty}^{\infty} P(y)(\overline{U}+u)^2\,dy = \overline{U}^2\int_{-\infty}^{\infty} P(y)\,dy + \int_{-\infty}^{\infty} P(y)u^2\,dy = \overline{U}^2 + u'^2,$$

Hence the second order moment is obtained as:

$$\mu^2 = 1 + I^2 \qquad (2.13)$$

2.1.3.2 Expression of the PDF Used in QBT

The PDF used in QBT is modified from Maxwell's PDF is by Çıray [6]:

$$P(y) = P(1)y^n exp\left[A^n\left(1-y^n\right)\right]\ . \qquad (2.14)$$

where $P(1)$ and A are constants that depends on the variable n. All of these coefficients are specific to case.

Then, PDF can be formed as:

$$P(y) = Cy^n exp\left(-A^n y^n\right) = C\varphi(y)\ , \tag{2.15}$$

where

$$C = P(1)exp(A^n)\ , \tag{2.16a}$$

$$\varphi(y) = y^n exp\left(-A^n y^n\right)\ . \tag{2.16b}$$

As the negative and positive fluctuations of the same magnitude may occur at different probabilities but at the same frequency, the PDF developed by Çıray is a skewed one. As PDF must represent the data accurately, it is important to choose the correct PDF. In Chapter 4, the PDF developed by Çıray is compared with histograms of the data to observe its power to represent the data precisely. In the following sections, how the coefficients of the PDF are obtained is explained.

2.1.3.3 Finding *P(1)*

Considering the property of PDF given as equation2.10a, the constant C given as equation2.16a can be written as:

$$C = \frac{1}{\int_{-\infty}^{\infty}\varphi(y)\,dy}\ . \tag{2.17}$$

To evaluate the integral in the denominator, following transformations are applied:

$$y^n = q \tag{2.18a}$$

$$dy = \frac{1}{n}\frac{q^{\frac{1}{n}}}{q}dq \tag{2.18b}$$

Then, the integral becomes:

$$\int_{-\infty}^{\infty}\varphi(y)\,dy = \int_{-\infty}^{\infty} y^n exp\left(-A^n y^n\right)\ dy = \int_{-\infty}^{\infty} qexp\left(-A^n q\right)\ \frac{1}{n}\frac{q^{\frac{1}{n}}}{q}dq\ .$$

Rearranging it, we arrive at:

$$\int_{-\infty}^{\infty}\varphi(y)\,dy = \frac{1}{n}\int_{-\infty}^{\infty} q^{\frac{1}{n}} exp\left(-A^n q\right)\ dq\ . \tag{2.19}$$

When the right-hand side of the equation is examined closely by Çıray, it is found similar to the definition of the Gamma function in the 'Handbook of Mathematical Foundations' book by Abramowitz [1][6]. Parallel to that, the terms in the right-hand side of equation 2.19are associated with the terms in the Gamma function[8]:

$$\Gamma(z) = k^z \int_0^\infty t^{z-1} exp\,(-kt)\ dt\ . \tag{2.20}$$

It can be observed that the lower limits of the integrals in the equations 2.19 and 2.20 are not the same. Since PDF is defined for $y \geq 0$, it does not cause any trouble and equation 2.19 can be expressed as:

$$\int_{-\infty}^{\infty} \varphi(y)\, dy = \int_0^\infty \varphi(y)\, dy \tag{2.21}$$

Thus, the correspondence between the terms of equation 2.19 and the Gamma function 2.20 can be introduced as below:

Table 2.1: Transformations for equations 2.19and 2.20

Equation 2.20		Equation 2.19
t	$\rightarrow$	q
k	$\rightarrow$	A^n
$z-1$	$\rightarrow$	$\frac{1}{n}$
z	$\rightarrow$	$\frac{n+1}{n}$

Applying those transformations given in the table 2.1, one can obtain:

$$\int_{-\infty}^{\infty} \varphi(y)\, dy = \frac{1}{n} A^{-(n+1)} \Gamma\left(\frac{n+1}{n}\right) \tag{2.22}$$

After that, equations 2.17 and2.16a brought together, C and $P(1)$ are obtained as:

$$C = \frac{nA^{n+1}}{\Gamma\left(\frac{n+1}{n}\right)}\ , \tag{2.23}$$

$$P(1) = \frac{nA^{n+1}}{\Gamma\left(\frac{n+1}{n}\right) exp(A^n)}\ . \tag{2.24}$$

Putting C and $P(1)$ into 2.15, PDF is obtained as:

$$P(y) = \frac{nA^{n+1}}{\Gamma\left(\frac{n+1}{n}\right)} y^n exp(-A^n y^n) \tag{2.25}$$

Besides, PDF can be written in terms of x by the same procedure and using the definition of y, ie., $y = 1 + Ix$:

$$P(x) = I\frac{nA^{n+1}}{\Gamma\left(\frac{n+1}{n}\right)} (1 + xI)^n exp\left[-A^n(1 + xI)^n\right] \ , \tag{2.26}$$

2.1.3.4 Finding *A*

If the property 2.10d is applied to 2.15 :

$$C\int_{-\infty}^{\infty} \varphi(y) y \, dy = C\int_{-\infty}^{\infty} y^{n+1} exp\left(-A^n y^n\right) \, dy = 1 \ . \tag{2.27}$$

Then, using the transformation $y^n = q$ given in the table 2.1 following equation is obtained:

$$C\int_{-\infty}^{\infty} q^{\frac{n+1}{n}} exp\left(-A^n q\right) \frac{1}{n}\frac{q^{\frac{1}{n}}}{q} \, dq = \frac{C}{n}\int_{-\infty}^{\infty} q^{\frac{2}{n}} exp\left(-A^n q\right) \, dq = 1 \ . \tag{2.28}$$

Table2.1 is used again for transformation of 2.28 except z and $z - 1$. A new transformation is applied for z and $z - 1$ as:

$$z = \frac{n+2}{n} \tag{2.29a}$$

$$z - 1 = \frac{2}{n} \tag{2.29b}$$

Using the transformations, following equation is found:

$$C\frac{1}{n}\Gamma\left(\frac{n+2}{n}\right)\frac{1}{A^{n+2}} = 1 \ . \tag{2.30}$$

And using equation 2.23, above relation yields to:

$$\frac{nA^{n+1}}{\Gamma\left(\frac{n+1}{n}\right)}\frac{1}{n}\Gamma\left(\frac{n+2}{n}\right)\frac{1}{A^{n+2}} = 1 \tag{2.31}$$

Therefore, A is obtained as:

$$A = \frac{\Gamma\left(\frac{n+2}{n}\right)}{\Gamma\left(\frac{n+1}{n}\right)} \ . \tag{2.32}$$

2.1.3.5 Finding μ^{κ}

The moment definition given in Eqn. 2.11, can applied to 2.15 and the resulting equation becomes:

$$\mu^{\kappa} = \frac{1}{\overline{U}^{\kappa}} \int_{-\infty}^{\infty} P(y) U^{\kappa} \, dy = \int_{-\infty}^{\infty} P(y) y^{\kappa} \, dy = C \int_{-\infty}^{\infty} y^{n} exp\left(-A^{n} y^{n}\right) y^{\kappa} \, dy \; .$$

Or,

$$\mu^{\kappa} = C \int_{-\infty}^{\infty} y^{n+\kappa} exp\left(-A^{n} y^{n}\right) \, dy \tag{2.33}$$

Again, using $y^{n} = q$ and $dy = \frac{1}{n} \frac{q^{\frac{1}{n}}}{q} dq$, one can arrive:

$$\mu^{\kappa} = \frac{C}{n} \int_{-\infty}^{\infty} q^{\frac{1+\kappa}{n}} exp\left(-A^{n} q\right) \, dq \; . \tag{2.34}$$

The transformation table for this relation is as follows:

Table 2.2: Transformation for equations 2.20and 2.34

Eqn. 2.20		Eqn. 2.34
t	$\rightarrow$	q
k	$\rightarrow$	A^{n}
$z-1$	$\rightarrow$	$\frac{1+\kappa}{n}$
z	$\rightarrow$	$\frac{n+\kappa+1}{n}$

Again, using the table 2.2 one can obtain:

$$\mu^{\kappa} = \frac{C}{n} A^{-(n+\kappa+1)} \Gamma\left(\frac{n+\kappa+1}{n}\right) \; . \tag{2.35}$$

Further, A and C constants expressed in terms of Gamma function before in 2.32 and 2.24 can be implemented to 2.35:

$$\mu^{\kappa} = \frac{\left[\Gamma\left(\frac{n+1}{n}\right)\right]^{\kappa-1} \Gamma\left(\frac{n+\kappa+1}{n}\right)}{\left[\Gamma\left(\frac{n+2}{n}\right)\right]^{\kappa}} \; . \tag{2.36}$$

If κ in the 2.36 is taken as two, the second moment can be obtained in terms of Gamma function and number n. Besides, it is known that $\mu^{2} = 1 + I$ by definition of

μ^2. Therefore:

$$\mu^2 = 1 + I^2 = \frac{\Gamma\left(\frac{n+1}{n}\right)\Gamma\left(\frac{n+3}{n}\right)}{\left[\Gamma\left(\frac{n+2}{n}\right)\right]^2} \ . \tag{2.37}$$

It is important to note that the equation 2.37 is used to find number n when the turbulence intensity I is known.

2.1.4 Discrete Form of Working Equations

In this section, the second main equation of QBT given in 1.19 is discretized. Having $x = u/u'$ in mind, 1.19 can be written as:

$$\int_{-\infty}^{\infty} P(x)x^2\,dx = \int_{0}^{\infty} G(f)\,df \ . \tag{2.38}$$

Since the PDF is skewed, through the discretization process, the left and right sides of the PDF are treated separately. Thus the equation becomes:

$$\int_{-x_{i+1}}^{-x_i} P_L(\xi)\xi^2\,d\xi + \int_{x_i}^{x_{i+1}} P_R(\xi)\xi^2\,d\xi = \int_{f_i}^{f_{i+1}} G(\eta)\,d\eta \ . \tag{2.39}$$

Here, dimensionless velocity ranges can be expressed as between $\pm x_i$ and $\pm x_{i+1}$. Hence, probabilities of the same velocity intervals is calculated separately, as they may differ for plus and minus fluctuations. However, as they occur at the same frequency, their contribution is calculated as a whole for a frequency range between f_i and f_{i+1}. This can be expressed in discrete form as follows:

$$\left[P_L(-x_{i+1})(-x_{i+1})^2 + P_L(-x_i)(-x_i)^2\right]\frac{-x_{i+1}-(-x_i)}{2} + \left[P_R(x_{i+1})(x_{i+1})^2 + P_R(x_i)(x_i)^2\right]\frac{x_{i+1}-x_i}{2} = \Delta G(f_i; f_{i+1}) \ . \tag{2.40}$$

By expanding $P_R(x_{i+1})$ and $P_L(-x_{i+1})$ according to first-order Taylor Series expansion one can get:

$$x_{i+1} = x_i + \Delta x_{i+1} \quad \rightarrow \quad P_R(x_{i+1}) = P_R(x_i) + \frac{dP_R(x_i)}{dx}\Delta x_{i+1} \ , \tag{2.41}$$

$$-x_{i+1} = -x_i - \Delta x_{i+1} \quad \rightarrow \quad P_L(-x_{i+1}) = P_L(-x_i) - \frac{dP_L(-x_i)}{dx}\Delta x_{i+1} \tag{2.42}$$

Plugging the expansions of $P_R(x_{i+1})$ and $P_L(-x_{i+1})$ into equation 2.40, the equation yields to:

$$\left\{\left[P_L(-x_i) - \frac{dP_L(-x_i)}{dx}\Delta x_{i+1}\right](-x_i - \Delta x_{i+1})^2 + P_L(-x_i)(-x_i)^2\right\}\frac{\Delta x_{i+1}}{2} + \left\{\left[P_R(x_i) + \frac{dP_R(x_i)}{dx}\Delta x_{i+1}\right](x_i + \Delta x_{i+1})^2 + P_R(x_i)(x_i)^2\right\}\frac{\Delta x_{i+1}}{2} = \Delta G(f_i; f_{i+1}). \tag{2.43}$$

Ignoring the terms of third order and more, following equation is arrived:

$$C_1\Delta x_{i+1}^2 + C_2\Delta x_{i+1} = \Delta G(f_i; f_{i+1}) \ , \tag{2.44}$$

where

$$C_1 = x_i\left[P_L(-x_i) + P_R(x_i)\right] + \frac{1}{2}x_i^2\left[\left.\frac{dP_L}{dx}\right|_{-x_i} + \left.\frac{dP_R}{dx}\right|_{x_i}\right] , \tag{2.45}$$

$$C_2 = x_i^2\left[P_L(-x_i) + P_R(x_i)\right] \ . \tag{2.46}$$

As can be seen from the equations 2.45 and 2.46, C_1 and C_2 values depend on the right and left PDF values and their derivatives. Also, after initiating the calculations with a specific x, Δx values can be found as the root of the equation2.44 .

2.1.5 Initiation of Calculation of Working Equations

In this section, the initiation of the calculations using an initial value, x_1, will be explained. Also, how the wavenumber k is found will be discussed.

2.1.5.1 Expression of x_1

For an initial value $x_0 = 0$, corresponding PDF values are:

$$P_L(x = 0) = P_R(x = 0) = P(1)$$

Also,

$$\int_0^{x_1} 2P(1)x^2\,dx = \Delta G(0; 1) \ , \tag{2.47}$$

where ΔG and $P(1)$ are constant. Therefore, x_1 can be found as:

$$x_1 = \left(\frac{3}{2}\frac{\Delta G(0;1)}{P(1)}\right)^{\frac{1}{3}} . \tag{2.48}$$

Subsequent x_i values can be found as

$$\mathrm{x}_{i+1} = x_i + \Delta x$$

where Δx is found from the equation 2.44. The results are in the form of $x = x(f)$

2.1.5.2 Expression of $k(f)$

In the previous chapter, first main equation of QBT is given as:

$$u = \frac{d\omega}{dk} .$$

This is the relation which is used to find wavenumber k. Keeping in mind that the circular frequency is defined as $\omega = 2\pi f$ and the nondimensional fluctuation velocity is given as $x = u/u'$, one can proceed to the relation:

$$k = \int_0^{\omega} \frac{d\omega}{u} = \frac{2\pi}{u'} \int_0^{f} \frac{df}{x} . \tag{2.49}$$

By splitting the integral, one can arrive at:

$$k(f) = \frac{2\pi}{u'} \left(\int_0^1 \frac{df}{x} + \int_1^f \frac{df}{x} \right) = k(1) + \frac{2\pi}{u'} \int_1^f \frac{df}{x} \tag{2.50}$$

Also, $x(f)$ can be expressed as:

$$x = x_b \left(\frac{f}{f_b}\right)^B , \tag{2.51}$$

where B, x_b, and f_b are available when the first three values of x and f are known. Therefore, $k(1)$ can be calculated as:

$$k(1) = \frac{2\pi}{u'} \frac{f_b^B}{x_b} \int_0^{f_1} \frac{df}{f^B} = \frac{2\pi}{u'} \left(\frac{f_b}{f_1}\right)^B \frac{f_1}{1-B} . \tag{2.52}$$

Inserting $k(1)$ into equation 2.50, one obtains:

$$k(f_i) = \frac{2\pi}{u'} \left(\frac{f_b}{f_1}\right)^B \frac{f_1}{1-B} + \frac{4\pi}{u'} \sum_{j=2}^{i} \frac{f_j - f_{j-1}}{x_j + x_{j-1}} \ . \tag{2.53}$$

or, in a simpler form:

$$k(f_i) = \frac{2\pi}{u'} \left[\left(\frac{f_b}{f_1}\right)^B \frac{f_1}{1-B} + 2 \sum_{j=2}^{i} \frac{f_j - f_{j-1}}{x_j + x_{j-1}} \right] \ . \tag{2.54}$$

After obtaining the wavenumber, k, wavelength, L, and the phase velocity, c can be obtained by employing the definitions $L = 1/k$ and $c = \omega/k$, respectively.

CHAPTER 3

METHOD

3.1 Introduction

In this section, the computer code developed in MATLAB for calculations based on QBT is explained in two subsections. In the first part of the code, Fourier transformations are carried out and the energy spectrum in frequency is obtained. The second part of the code deals with the constructing PDF function and wave number.

3.2 First Part: Fourier Transforms

This section aims to obtain energy contributions of some frequency ranges utilizing Fourier transforms.

3.2.1 inputs

Inputs of this part of the code are the data of the instantaneous velocity fluctuations, sampling time T, size of the data N, and sampling rate F_s

3.2.2 $'fft'$ command

Matlab has $'fft'$ command to execute the Fast Fourier Transform(FFT). As explained before, FFT gives results faster compared to DFT. Fourier transform aims to represent a function in the frequency domain where the function is previously defined in the time domain. In our case, discretized data is used instead of a continuous function.

Fourier transformations, therefore, are performed using the command $fft(d)$, where ,d is a column vector that includes the fluctuating components of the instantaneous velocities. The output of this command is a vector of the same size as d, but the values are complex numbers. The Fourier coefficients $a(f)$ and $b(f)$ can be found as the imaginary part and the real part of the complex value, respectively.

3.2.3 Energy Densities

After obtaining Fourier coefficients, the discrete form of equation1.3 is employed to find the energy densities contained in corresponding frequency values:

$$E(f) = \frac{a^2 + b^2}{F_s} \tag{3.0}$$

E(f) here, is the spectral density function. At this stage, when the $E(f)$ values are plotted with respect to frequency, using an appropriate frequency vector, a symmetrical two-sided spectrum is obtained. This result springs from the fact that $'fft'$ includes some negative frequency values, which are physically meaningless but the contributions of which should be taken into account. Thus, a one-sided spectrum that has meaningful frequency values and accurate energy densities are desired. To do that, one side of the spectrum is added to the other side of the spectrum. This means that the energy densities for one side are doubled as the two-sided spectrum is a symmetrical one. This is done by forming vectors for energy densities as:

$$E1 = E2(1 : T/2 + 1)$$

$$E1(2 : end - 1) = 2 * E1(2 : end - 1)$$

where E1 is the vector containing energy densities corresponding to the two-sided spectrum obtained in the beginning and E2 is the new vector corresponding to one-sided spectrum. Accordingly, a convenient frequency vector is formed as:

$$f = F_s * (0 : (T/2))/T$$

Here, the maximum frequency value is chosen as half of the sampling rate in accordance with the Nyquist criteria.

3.2.4 Integration and Nondimensionalization of Energy Densities

To represent the energy contribution of eddies, twelve frequency values are chosen as 1, 2, 5, 10, 20, 50, 100, 200, 500, 1000, 2000, and 5000 [6]. Energy contributions for the ranges between those values (1-2 Hz,2-5 Hz,5-10 Hz, etc.) are calculated by computing the trapezoidal area corresponding to those frequency ranges and they are called ΔG. As the area under the spectrum must be equal to one, a nondimensionalization of the energy densities is required. To do that, energy densities are divided by the square of the rms of the fluctuation velocities and also by the sampling rate and the number of samples:

$$E(f) = \frac{1}{N}\frac{a^2 + b^2}{rms^2}\frac{1}{F_s}, \tag{3.0}$$

Therefore, as the output of this section we have energy densities ΔG for the specified ranges of frequency.

3.3 Second Part: The PDF

In this section, finding the n number, the second moment of PDF, the right and left PDF values and the PDF as a function will be discussed in detail.

3.3.1 Inputs

For this part of the code, ΔG values obtained from the first part of the code are used as input in the form of a vector of size twelve. Also, mean velocity for a measurement point and root mean square of the velocity fluctuations are used as input values as well. From those values, it is possible to find the turbulence intensity as it is defined as $I = u'/\overline{U}$. Besides, the second moment is calculated as $\mu^2 = 1 + I^2$, this is called I_{act} where the subscript $'act'$ stands for 'actual'.

3.3.2 Finding μ^2 and n

Other than the I_{act} value, calculated from the data itself, the code also finds a μ^2 value in terms of Gamma function, as defined in 2.37. From this second μ^2 value, a new

turbulence intensity, I_{calc}, is found, where $'calc'$ stands for 'calculated'. The code aims to equate I_{calc} to I_{act}. To do that, two loops in nested form are used. While the inner loop performs the calculations for I_{calc} using the n number iteratively, the outer loop checks the error defined as $I_{act} - I_{calc}$ for each iteration. The error is defined such that it is smaller than 0.000001. If the error is found larger than this value, calculations will be performed by using a smaller step size for number n. Thus, the appropriate number n is found.

3.3.3 Finding PDF

After dealing with μ^2, calculations for the PDF is initialized by:

$$P_L(x = 0) = P(1)$$
$$P_R(x = 0) = P(1)$$

where $x_0 = 0$ p(1) is given in 2.26:

$$P(1) = \frac{nA^{n+1}}{\Gamma\left(\frac{n+1}{n}\right)exp(A^n)}$$

For the positive and negative values of x, two vectors are formed and named as X and x_n. The values of them are the same in magnitude but opposite in signs. Similarly, corresponding y and y_n vectors are defined as:

$$y = 1 + Ix$$
$$y_n = 1 + Ix_n$$

y values are used for calculation of the right side of the PDF, denoted as PDF_R and y_n is used to find the values for the left side of the PDF, denoted as PDF_L.

Recalling equation 2.48 x_1 and $-x_1$ are found as:

$$x_1 = \left(\frac{3}{2}\frac{\Delta G(0;1)}{P(1)}\right)^{\frac{1}{3}}$$
$$-x_1 = -\left(\frac{3}{2}\frac{\Delta G(0;1)}{P(1)}\right)^{\frac{1}{3}}$$

Then, constant C is calculated according to equation 2.23 :

$$C = \frac{nA^{n+1}}{\Gamma\left(\frac{n+1}{n}\right)}$$

After that, PDF_R and PDF_L is calculated from the equation 2.15 :

$$PDF_R(y) = Cy^n exp\left(-A^n y^n\right)$$
$$PDF_L(y) = Cy_n^n exp\left(-A^n y_n^n\right)$$

Then, derivatives of left and right PDFs are also calculated for the calculation of $C1$ and $C2$ parameters:

$$DPDF_R = -(I^2 CNy^(N-1)exp(-A^N y^N))(1 + y^N(-A^N))$$

$$DPDF_L = -(I^2 CNy_n^(N-1)exp(-A^N y_n^N))(1 + y_n^N(-A^N))$$

Using 3.3.3 and 3.3.3 $C1$ and $C2$ can be found from the equations 2.45 and 2.46

$$C_1 = x_i\left[PDF_L(-x_i) + PDF_R(x_i)\right] + \frac{1}{2}x_i^2\left[DPDF_L\Big|_{-x_i} + DPDF_R\Big|_{x_i}\right]$$

$$C_2 = x_i^2\left[PDF_L(-x_i) + PDF_R(x_i)\right]$$

Finally, dx is found from the equation 2.44 and it is used for the next value in the x and x_n vectors:

$$dx(i) = (-C_2 + sqrt(C_2.^2 + 4 * C_1 * DG(i+1)))/(2 * C_1)$$

$$X = X + dx(i)$$

$$Xn = Xn - dx(i)$$

where DG is the vector for the energy densities obtained from the first part of the code.

3.3.4 Finding k

Recalling the equations 2.52 and 2.51 given in the previous chapter, first three x and f values are needed for calculation of B parameter:

$$B = log(X(3)/X(2))/log(F(2)/F(1))$$

Also,

$$XA = X(3)/(F(2)^B)$$

Therefore, first two k values are found as:

$$k(1) = 2\pi F(1)/(rmsXA(1-B))$$

$$k(2) = 2\pi F(2)/(rmsX(1-B))$$

where rms is root mean square.

And finally, subsequent values of k using equation 2.54 can be found as:

$$k(i) = k(i-1) + 2\pi((F(i) - F(i-1))/(rmsX(i)))$$

3.3.5 Verification of the code

In order to check whether the code produces the results in accordance with the mathematics of QBT, data from Çıray's study in 1980 is examined[6]. In the study, there are 10 different test cases and for each of them, energy densities corresponding to chosen frequency intervals are known. Results from Çıray's study in 1980 and results obtained using the code developed in this thesis study are compared and turn out to be very similar. Therefore, the code in this thesis study is verified and used for the analysis of two different experimental data.

CHAPTER 4

RESULTS

4.1 On Experimental Results

In this section, two different experiments are introduced. After explaining the setup and procedure of the experiments, results obtained by analyzing the data of these experiments are discussed in detail.

4.2 Micro Vortex Generator Experiment

4.2.1 Introduction

Micro vortex generators (MVG) are simple devices used to form small vortices in the flow field. They have a simple geometry of a ramp or a vane. MVG mixes the lower and upper regions of the boundary layer and therefore energy is transferred from upper to lower regions. As a result, the kinetic energy of the lower portions is increased and a more energetic boundary layer is produced. Hence, the use of MVG devices is an effective method for delaying separation[20]. The MVG experiment that will be mentioned in this section of this thesis is conducted by Akpolat for his Ph.D. research in progress and carried out at METU Center for Wind Energy (RÜZGEM). By kind permission of Akpolat, the data obtained from this experiment is used following the aims of this thesis.



Figure 4.1: METUWIND/RÜZGEM C3 Medium Scale Suction Type Wind Tunnel (adapted from[2])

h[mm]	w[mm]	c[mm]	α[°]
30	184	212	8.3

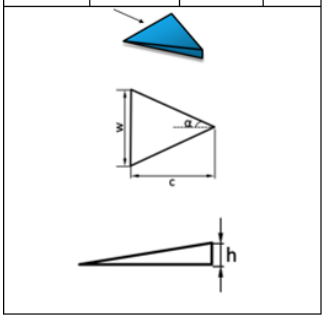


Figure 4.2: Dimensions and Geometry of MVG (adapted from [2])

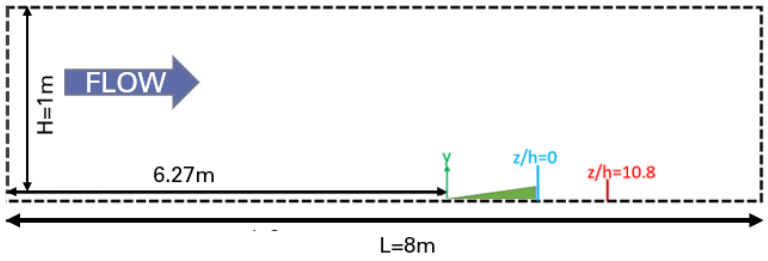


Figure 4.3: Placement of MVG (adapted from [2])

4.2.2 Setup and Method

The experiment is conducted in METUWIND/RÜZGEM C3 Medium Scale Suction Type Wind Tunnel. The free stream velocity is chosen as 10 m/s. The MVG) is located 6.2 m from the inlet of the tunnel. Hot Wire Anemometer (HWA) measurements were carried out at 324 mm downstream of the MVG, corresponding to z/h=10.8

The figure 4.2 shows the dimensions and the geometry of the MVG used in this experiment. In the figure 4.3 MVG placement inside the tunnel is demonstrated. The height of the tunnel is 1 m and the length of the tunnel is 8 m. MVG is placed 6.27 m

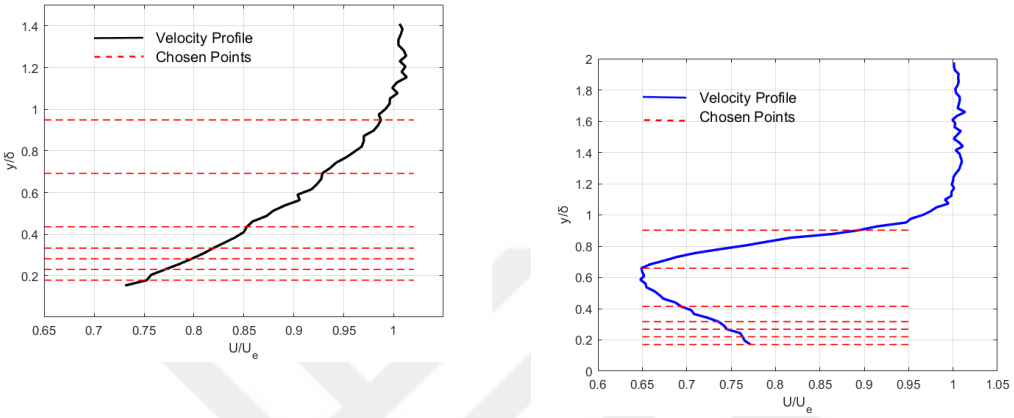
away from the tunnel inlet. z/h =0 point represents the corner of the MVG device and z/h=10.8 represents the point where the measurements are taken. The boundary layer probe employed for the measurements was placed 10 mm away from the bottom wall of the wind tunnel. The probe was traversed vertically up to 162 mm with increments of 2 mm for each measurement. The sampling time was chosen to be 30 s with a sampling frequency of 10 kHz.There are no measurements for 12 mm and 112 mm positions. Thus, the data is obtained for 74 different points. The same measurement procedure is repeated in the same wind tunnel without an MVG for the same traverse points on the 6.2 m distance from the inlet, as in the first case. Thus, undisturbed boundary layer data is also obtained[2]. From now on, these two cases will be called as 'MVG case' and 'Undisturbed Case'.

4.2.3 Analysis

For the analysis, 7 different measurement points are chosen: 14 mm, 18 mm, 22 mm, 26 mm, 34 mm, 54 mm, and 74 mm. The Analysis is carried out for both the Undisturbed case and the MVG case. For both cases, boundary layer velocity profiles are plotted for each chosen measurement point. Then, using the aforementioned method of QBT, PDFs, and histograms of chosen measurement points are obtained. Also, energy spectra based on frequency and wavenumber are obtained for each measurement point, again, for both cases. Since the sampling rate is 10 kHz, the maximum meaningful frequency is taken as 5000 Hz, in accordance with Nyquist criteria. For simplicity, plots corresponding to 4 measurement points will be demonstrated in the figures.

4.2.4 Results

First of all, boundary layer velocity profiles for both cases are obtained as in the below figures, where red dotted lines show the chosen data points. Also, boundary layer thickness for the undisturbed case is calculated as 78 mm whereas for the MVG case it is 88 mm.



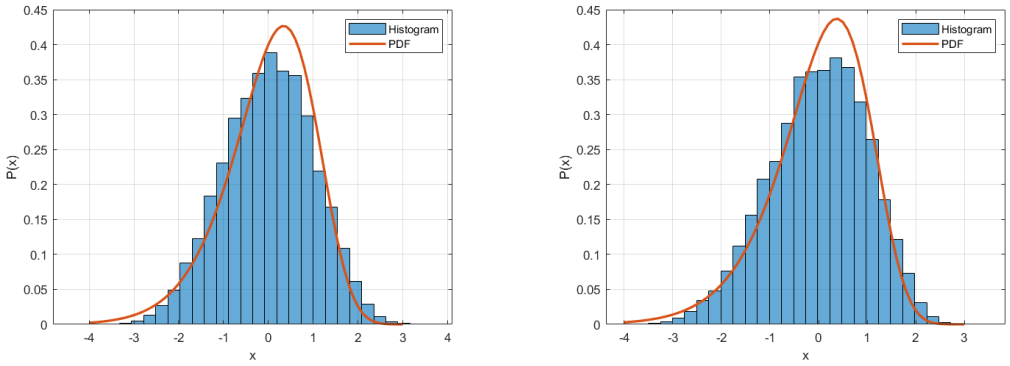
(a) (b)

Figure 4.4: Velocity profiles for the Undisturbed case(a) and for the MVG case(b)

From the figure4.4, a wake behind the MVG can be observed in the lower regions of the boundary layer, below 54 mm. Also, at 74mm, the boundary layer thickness is almost achieved for both cases. For the first 4 points, the velocity profile does not show a significant change in shape, thus analysis for only 14mm, 34 mm, 54 mm, and 74 mm will be shown in the plots.

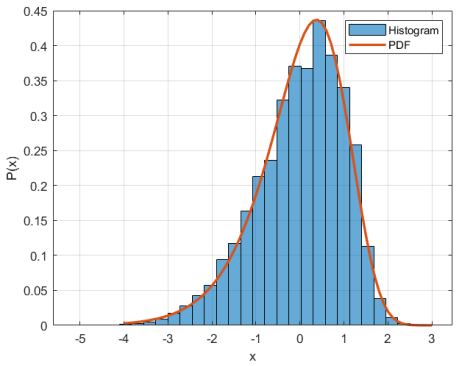
Secondly, probability density functions(PDF) for each point are obtained and compared with the histograms corresponding to the same point in order to observe their compatibility. Here, the aforementioned PDF function modified by Çıray[6] is used. On the horizontal axis, dimensionless velocity fluctuations are represented by x where P(x) shows the probability of corresponding fluctuations. Similarly, Histogram is obtained from the experimental data directly by using Matlab and normalized to be comparable with PDF. In a likewise manner, blue columns in the figures represent the probability of velocity fluctuations. Since histograms are obtained directly from the experimental data, this comparison shows us how precisely PDF represents the

experimental data.

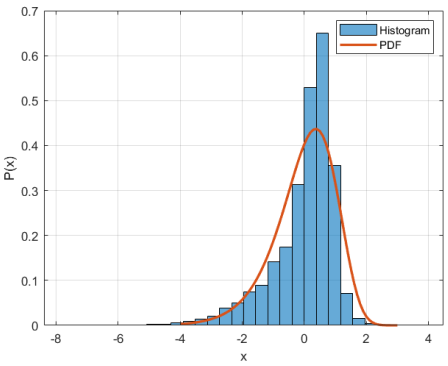


(a)

(b)



(c)



(d)

Figure 4.5: PDFs and Histograms for the Undisturbed Case at 14mm(a), 34mm(b), 54mm(c), 74mm(d)

Those four figures above are obtained for the Undisturbed case and for 14 mm, 34 mm, 54 mm, and 74 mm, respectively. From the figures 4.5a and 4.5b, it can be concluded that for the first two points, PDFs are compatible with the histograms. However, for 54 mm, PDF fits the histogram best. Thus, experimental data is represented most precisely for 54 mm. On the other hand, for the last point, 74 mm, which is the closest to boundary layer thickness, fluctuations around x=0 are underestimated by the PDF.

For the MVG case, same procedure is applied and plots are obtained as follows:

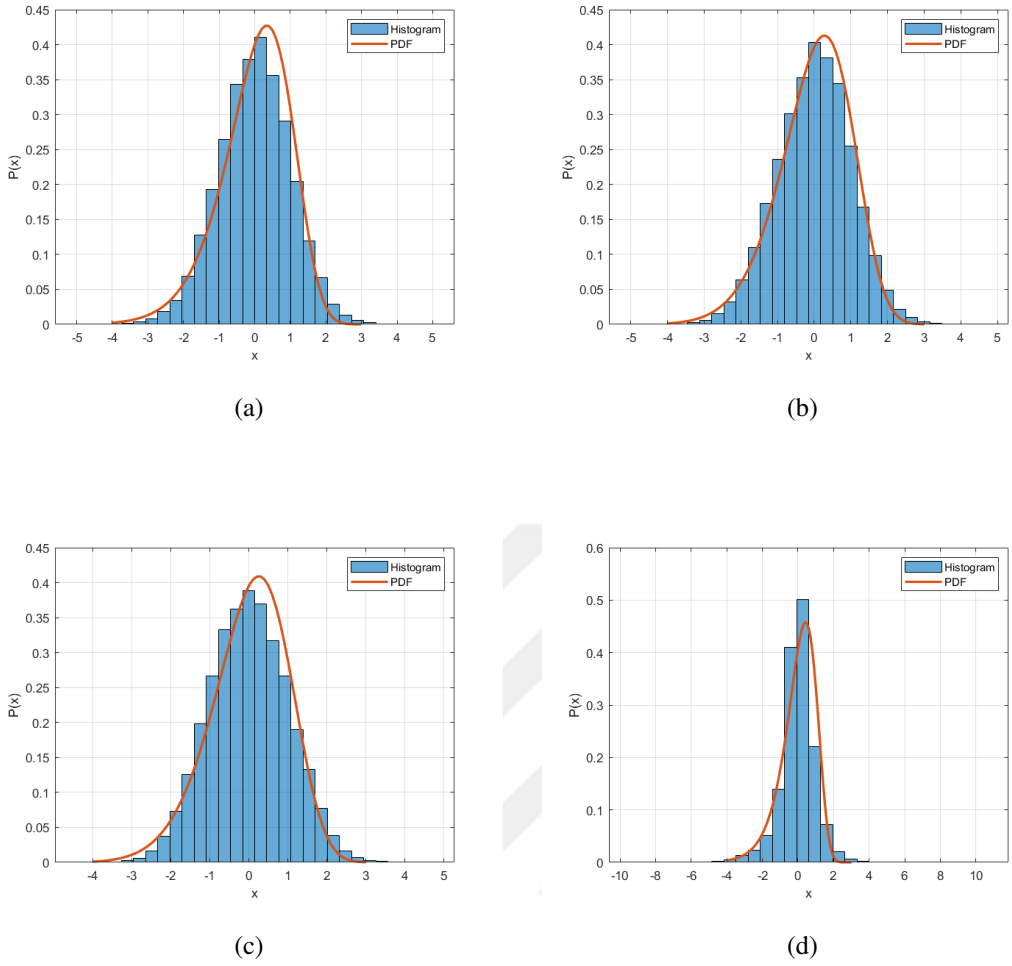


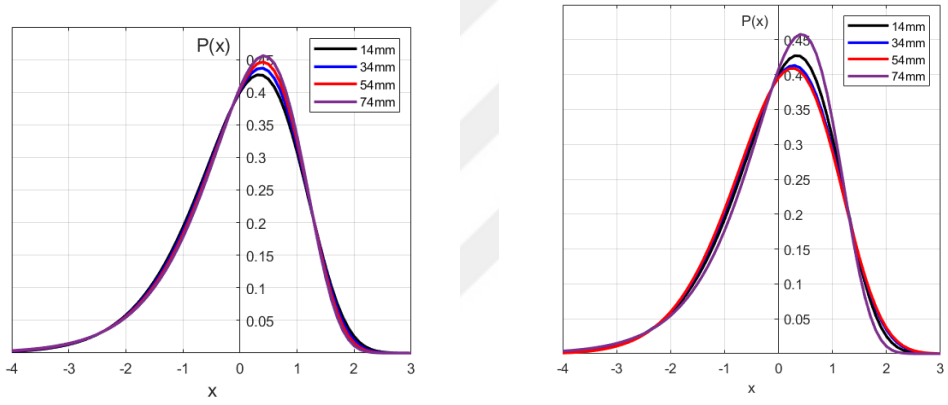
Figure 4.6: PDFs and Histograms for the MVG Case at 14mm(a), 34mm(b), 54mm(c), 74mm(d)

Similar to the Undisturbed case, data of the MVG case is well represented by the PDFs. Again, for 74 mm, there is an inconsistency between PDF and Histogram, but PDF fits better compared to the Undisturbed case for the same point. Also, skewness of the PDFs can be observed from the figures and it is mostly compatible with Histograms.

In order to compare the PDFs of different points, they plotted together, again for both cases. Figure 4.7 shows the PDFs at 14 mm, 34 mm, 54 mm, and 74 mm for the Undisturbed case.

From the figures, it can be observed that the probability of the fluctuations is highest around x=0.5. From both figures, it can be inferred that probabilities around the peak location increase constantly with the increasing distance from the solid boundaries within the boundary layer. For the larger dimensionless fluctuations, probabilities are quite similar for those four points.

Unlike the Undisturbed case, behavior of PDFs for the MVG case is not straightforward. That is, a constant increase in probabilities with increasing distance cannot be observed. If two figures are compared, it can be seen that while probabilities at the peak location for 14 mm and 74 mm do not change much, those for 54mm and 34mm are decreased in the presence of MVG. This is compatible with the velocity profile for the MVG case.



(a) (b)

Figure 4.7: PDFs for chosen points for Undisturbed Case(a) and for the MVG Case(b)

Another important part of the analysis is obtaining spectra based on wave number and frequency. In the figure 4.8, spectra based on wave number in logarithmic scale for all chosen points and for both cases are demonstrated.*G(k)* on the vertical axis is nondimensionalized energy density function. Here, the same colors represent the same point and dashed lines represent the MVG case where full lines represent the Undisturbed case. As mentioned in the earlier chapters, wavelengths represent the eddie sizes. Large wavenumbers correspond to large eddies, which are formed near the boundaries where large velocity gradients are present, and smaller wave numbers correspond to smaller eddies. Considering the definition of wavenumber, it can be

inferred that smaller wave numbers correspond to large eddies, and large wavenumbers correspond to smaller eddies. Based on that, it can be observed from the figure 4.8 that larger eddies are formed near the rigid boundaries. Spectra for 14mm point begins at much smaller wave numbers than the spectra for the 74 mm point for both cases. Also, in the large eddies region, the same wave number interval corresponds to higher energy for the Undisturbed case than the MVG case, for almost all points. On the contrary, for the universal equilibrium region, for the same wavelength interval, energies for the MVG case are higher than the Undisturbed case for all points. In the energetic eddies region, the highest energy is observed at 54mm and the lowest energy densities occur at 74 mm for MVG case. At the inertial subrange, it is possible to observe a -5/3 slope for both cases. This shows us the spectra obtained are compatible with the literature.

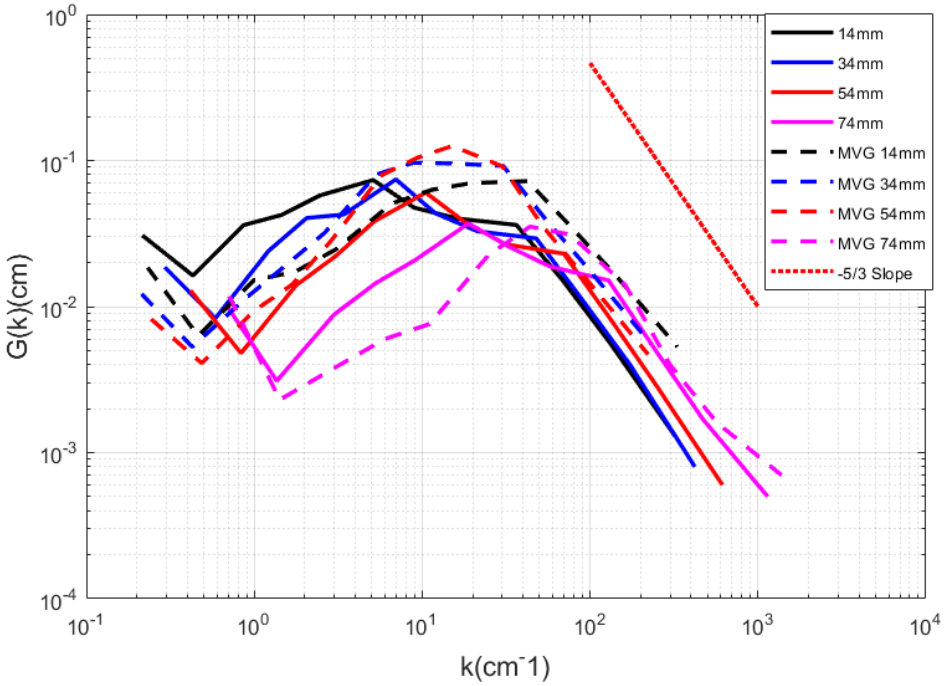


Figure 4.8: Spectra based on Wave Number in Logarithmic Scale for Both Cases

Figure 4.9 on the other hand, shows the spectra based on frequency for both cases.*G(f)* on the vertical axis is the nondimensionalized energy density function. Again, the same colors represent the same point, and dashed lines represent the MVG case where full lines represent the Undisturbed case. As a first observation, it can be seen that for

each point and almost for all frequency ranges, the MVG case has higher energy densities than Undisturbed case. Also, most of the contribution comes from the 0-2000 Hz range for both cases. When the distance from the solid boundaries is increased, a constant decrease in energy densities can be observed for the frequency interval between 200 and 1500 Hz for Undisturbed case. However, for MVG case, a direct relation between the distance from the wall and energy densities cannot be inferred at the same frequency range. There is no direct relation between the distance from the wall and energy densities can be inferred. This situation can be explained by the fact that MVG mixes the upper and lower portions of the flow within the boundary layer.

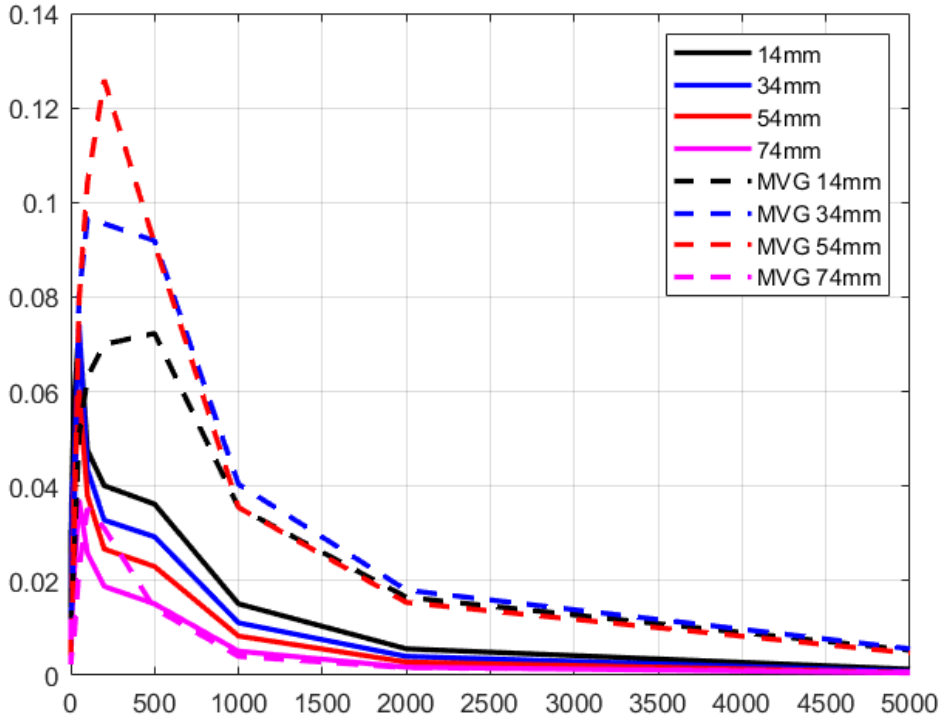


Figure 4.9: Spectra based on Frequency for Both Cases

From the table 4.1 the largest wavelength is 4.6361 cm and 4.3137 cm for the undisturbed case and MVG case, respectively. This is a significant result since the wavelength represents the eddy size and the largest eddy size must be reasonable when the physical boundaries of the experiment are considered. The boundary layer thickness can be taken as the dimension for the physical domain for these experiments and they

are 88 mm and 78 mm for the MVG case and undisturbed case, respectively. Thus, the largest eddies are smaller than the physical boundaries of the experiment for each case. This shows that QBT can predict physically meaningful eddy sizes.

Traverse Position(mm)	Largest Wavelength(cm)		Turbulence Intensity(-)		Mean Velocity(m/s)	
-	Undisturbed	MVG	Undisturbed	MVG	Undisturbed	MVG
14	4.6361	4.3137	0.0991	0.0975	7.7533	7.7533
34	3.4106	4.6859	0.0731	0.1404	8.7846	8.7846
54	2.3992	4.1116	0.0516	0.1541	9.5629	9.5629
74	1.4689	1.4117	0.0311	0.0269	10.1677	10.1677

Table 4.1: Comparison of undisturbed and MVG cases based on largest wavelength, turbulence intensity and mean velocity

The effect of MVG can be observed from the largest wavelengths listed for each case. As expected, there are larger eddies near the boundaries, i.e. the bottom wall of the tunnel for the Undisturbed case. Parallel to that, there is a continuous decrease in wavelength with increasing traverse position for the Undisturbed case. However, for the MVG case first, there is a decrease in wavelength up to 22 mm traverse position, then wavelength increases up to 54 mm position. It means that larger eddies are produced in respectively upper regions when MVG is employed. This phenomenon can be explained by the fact that MVG is a device that mixes the upper and lower layers of the flow.

4.3 The Experiment of Unconfined and Non swirling Jet

In this section, an experiment carried out using an unconfined and non-swirling jet is introduced and the results of the analysis of the data obtained from this experiment are discussed.

4.3.1 Setup and Method

In this experiment, flow behind a non-swirling jet with a circular cross-section for an unconfined case is studied. The outlet diameter of the jet is 28 mm and data is collected by using Hot Wire Anemometry at three different locations downstream of the jet, namely 0.3, 0.5, and 1 times the diameter. For each of these locations, hotwire probes are traversed by an increment of 1mm for an interval of 3.4 cm for only one side of the jet as the two sides are symmetric in terms of pressure and velocity measurements. The locations of measurements are depicted in the figure4.11. The mass flow rate at the exit is 6.8 g/s and the density of the air is 1.05 kg/m^3. Reynolds number is calculated as 17000 based on the hydraulic diameter and mean jet exit velocity, which is 10 m/s. The experiments are carried out at the Center for Wind Energy Research (RÜZGEM) of Middle East Technical University. The setup consists of a compressor, which is capable of maximum pressure of 14 bars, a pressurized air tank, a demoisture system, a coriolis type flow meter, and a settling chamber. After the air is compressed and demoisturized, it goes through a Coriolis-type flow meter and enters a manifold of four outlets. And finally, air is brought to the settling chamber and to the test section[16]. The experiment is carried out by Fırat Kıyıcı and Battal Gencer and by their kind permission, the data obtained from the experiment is used in this study.

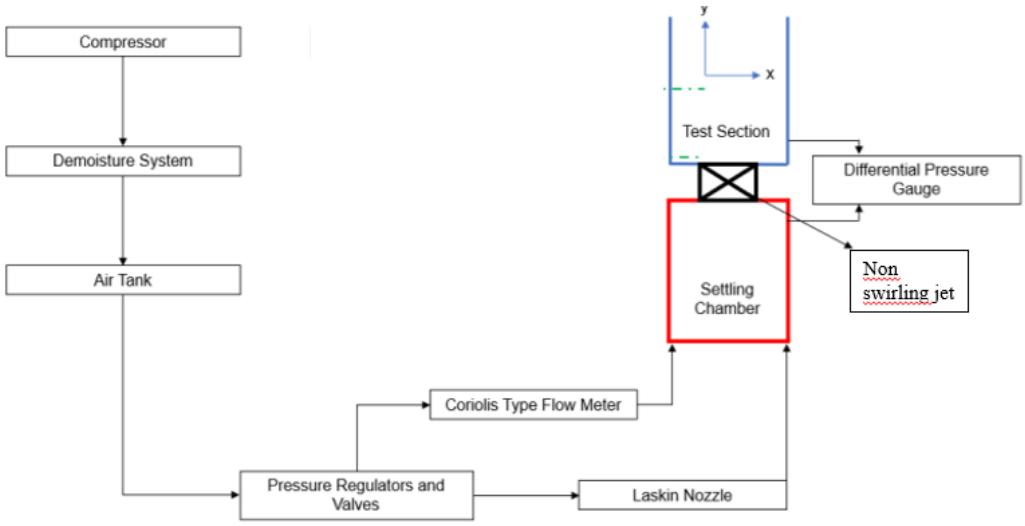


Figure 4.10: Schematic of the Non-swirling and Unconfined Jet Experiment Setup(adapted from [16])

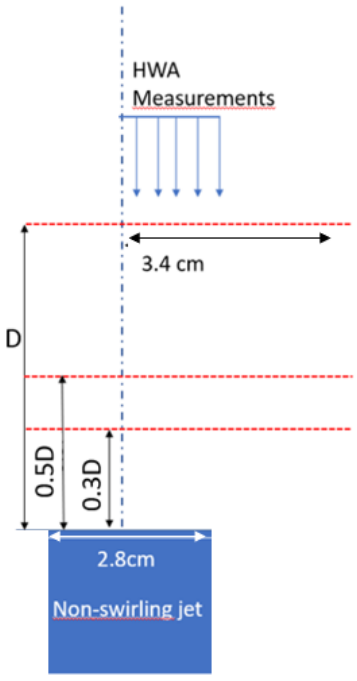


Figure 4.11: Measurement points for the Non-swirling and Unconfined Jet Experiment

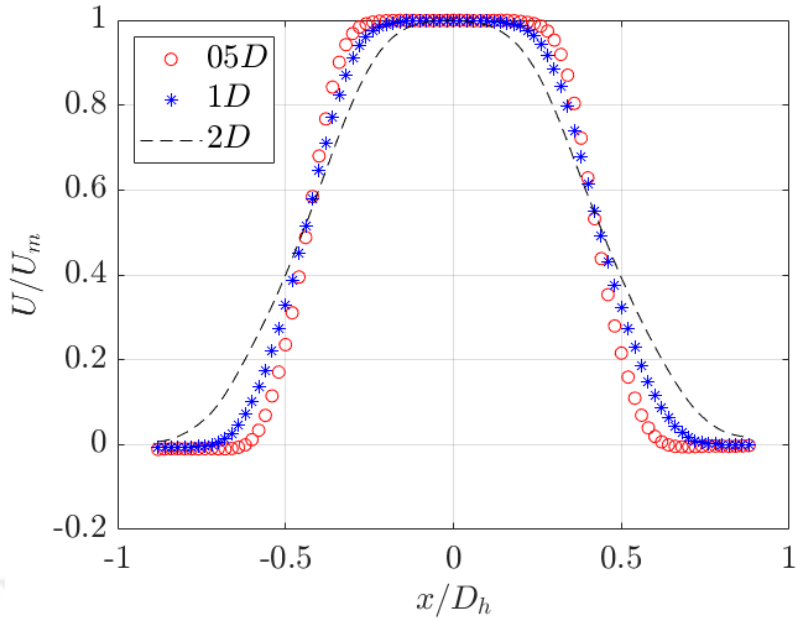


Figure 4.12: Symmetrical Velocity Profiles for the Non-swirling and Unconfined Jet Experiment

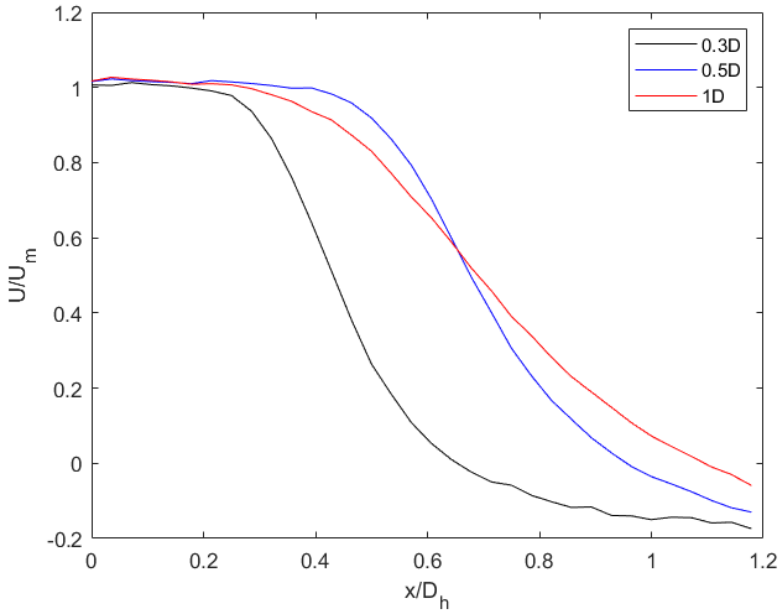


Figure 4.13: One-sided Velocity Profiles for the Non-swirling and Unconfined Jet Experiment

As can be seen from the figure 4.12, velocity profiles are obtained for 0.5D, 1D and 2D locations and it is observed that the profiles are symmetric. After observing the the symmetry, 0.3D ,0.5D and 1D locations are chosen for the analysis and data is obtained for 0.3 D location as well. However, for simplicity, only one half of the jet flow is studied for the analysis. Therefore, one-sided velocity profiles used for this analysis are as follows:

For 0.3D location the traverse locations above 18mm, HWA measurements contains minus values. This may be caused by the fact that in these regions velocities are small and calibration of the jet cannot work appropriately for these regions. Also, the analysis gives complex results for the 18 mm traverse position because of the same reasons. Thus, for 0.3 D location, 0 mm, 6mm, 10 mm, and 14 mm are chosen for the analysis. On the other hand, for 0.5 D and 1D locations, 18 mm can be analyzed without any complex results but above this point, meaningful results cannot be obtained. Therefore, at 0.5D and 1D locations 0 mm, 6mm, 10 mm, 14 mm, and 18 mm traverse positions are chosen for the analysis.

In figure 4.13 velocity profiles for each location are demonstrated. Since the velocity profile is symmetric around the jet, only one half of the velocity profile is used for analysis. In the following sections analysis of data at each traverse position and for each location is shown and results are discussed. Then, the results of three locations are compared.

4.3.2 PDFs and Histograms

Using the same procedure defined for the MVG experiment, probability density functions(PDF) and histograms are obtained for each traverse point and compared with each other to observe whether the PDFs fit to the histograms well. Once again, PDF modified by Çıray [6] is used. Similarly, Histogram is obtained from the experimental data directly by using Matlab and normalized to be comparable with PDF.

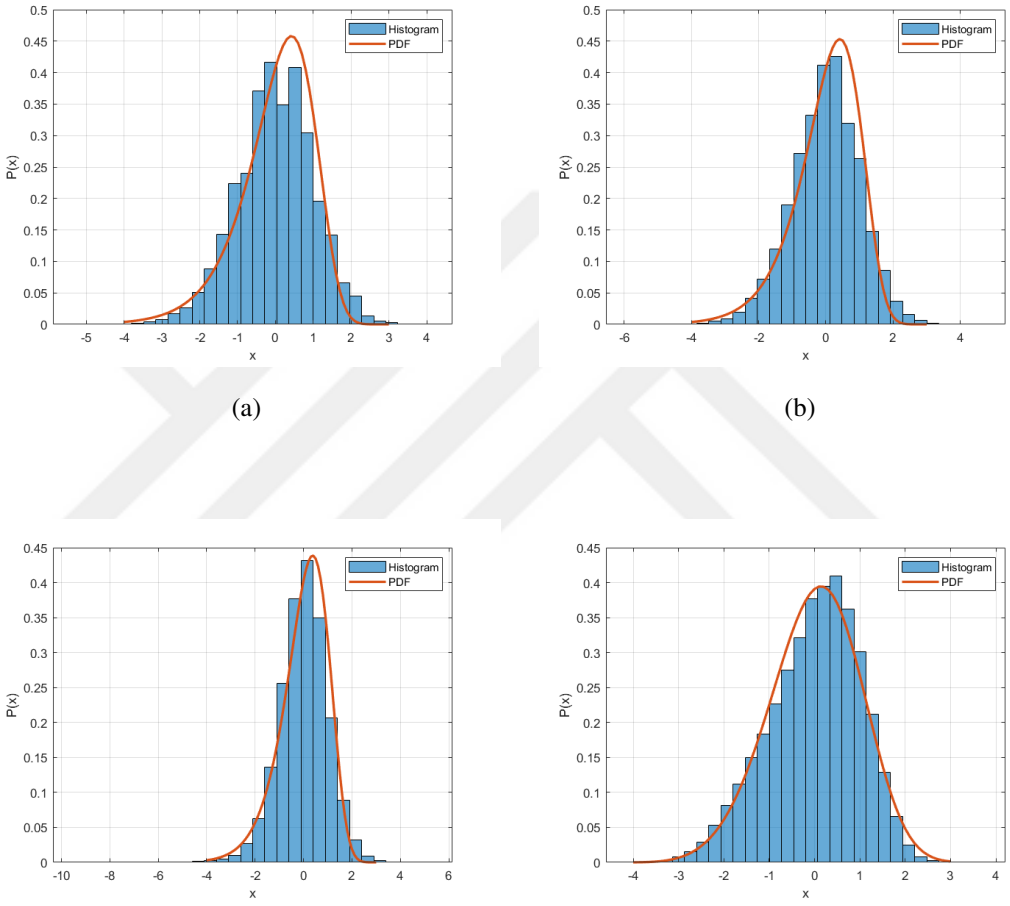


Figure 4.14: PDFs and Histograms for 0.3D Location at 0mm(a), 6mm(b), 10mm(c), 14mm(d).

For 0.3D Location, points above 14mm cannot give realistic results and above 18mm data contains minus values Therefore, PDFs and Histograms are obtained for 0mm, which corresponds to jet center, 6 mm, 10 mm, and 14 mm. Above figures demon-

strate the PDFs and histograms for 0.3D location. According to the figures it can be inferred that the PDF represents the experimental data well as it mostly fits the histograms.

Following figures show the PDFs and histograms for 0.5D and 1D location.

For 0.5D location, results for 18 mm traverse point are obtained as well. It is observed that for 10mm, 14 mm, and 18mm points, PDFs fit histograms better. It can be seen that, unlike others, the PDF for the 18mm traverse position has a more symmetrical distribution. The histogram of the corresponding point is also more symmetrical while at other points, histograms are more skewed in general. Also, it can be observed that for the 0mm, that is the jet center, the histogram is more symmetric while PDF predicts a left-skewed distribution.

Lastly, PDFs and Histograms are obtained for the 1D location. Again, 18mm point can be analyzed at this location. It can be observed from the below figures that the PDFs fit histograms for 10mm and 14mm better than the other points. However, for 18mm point, PDF is more symmetrical than the histogram and the histogram has a right-skewed distribution. Moreover, similar to the one for 0.5D location, the histogram for 0mm is more symmetrical than the PDF for the corresponding point.

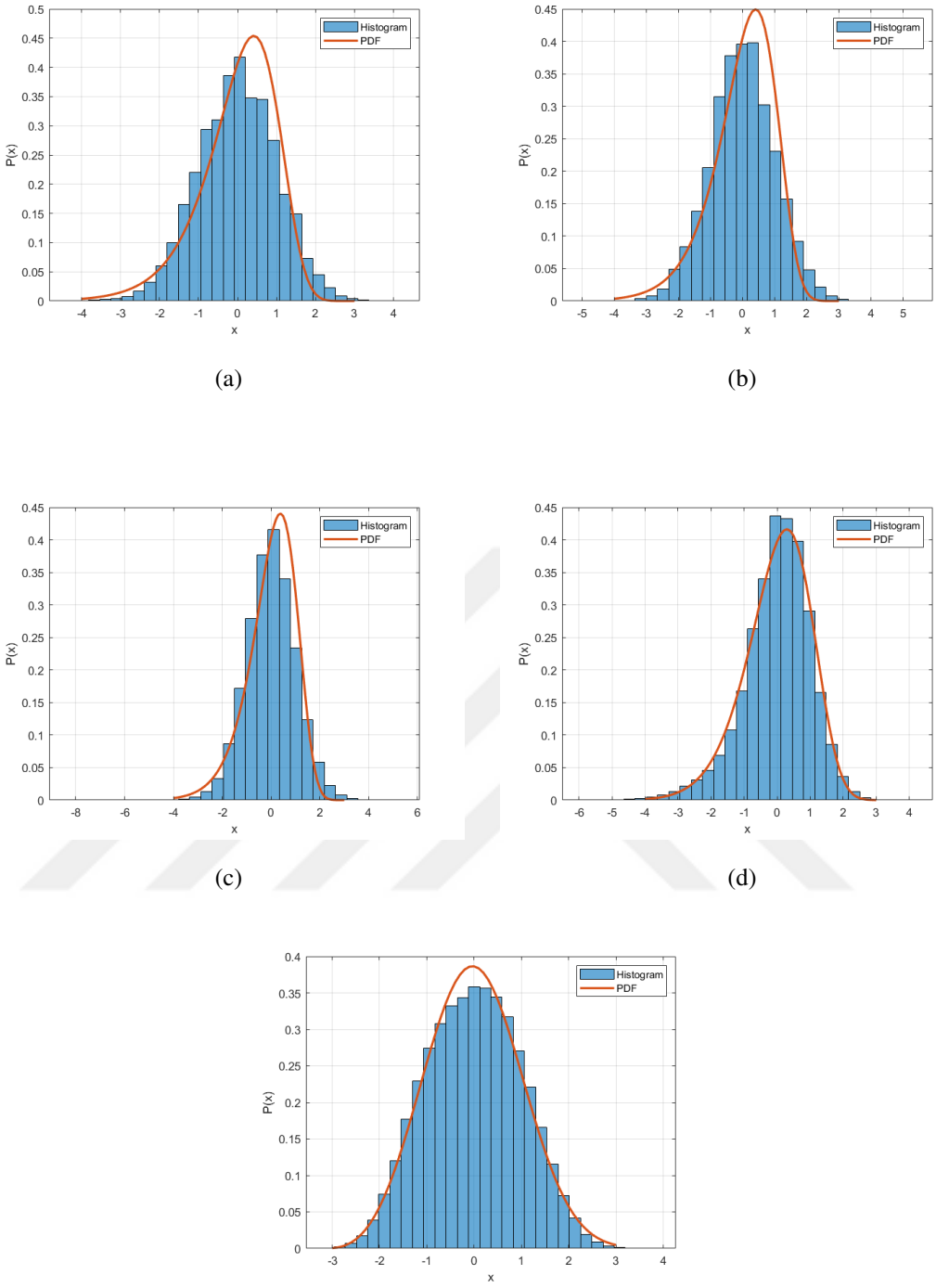


Figure 4.15: PDFs and Histograms for 0.5D Location at 0mm(a), 6mm(b), 10mm(c), 14mm(d), 18mm(e).

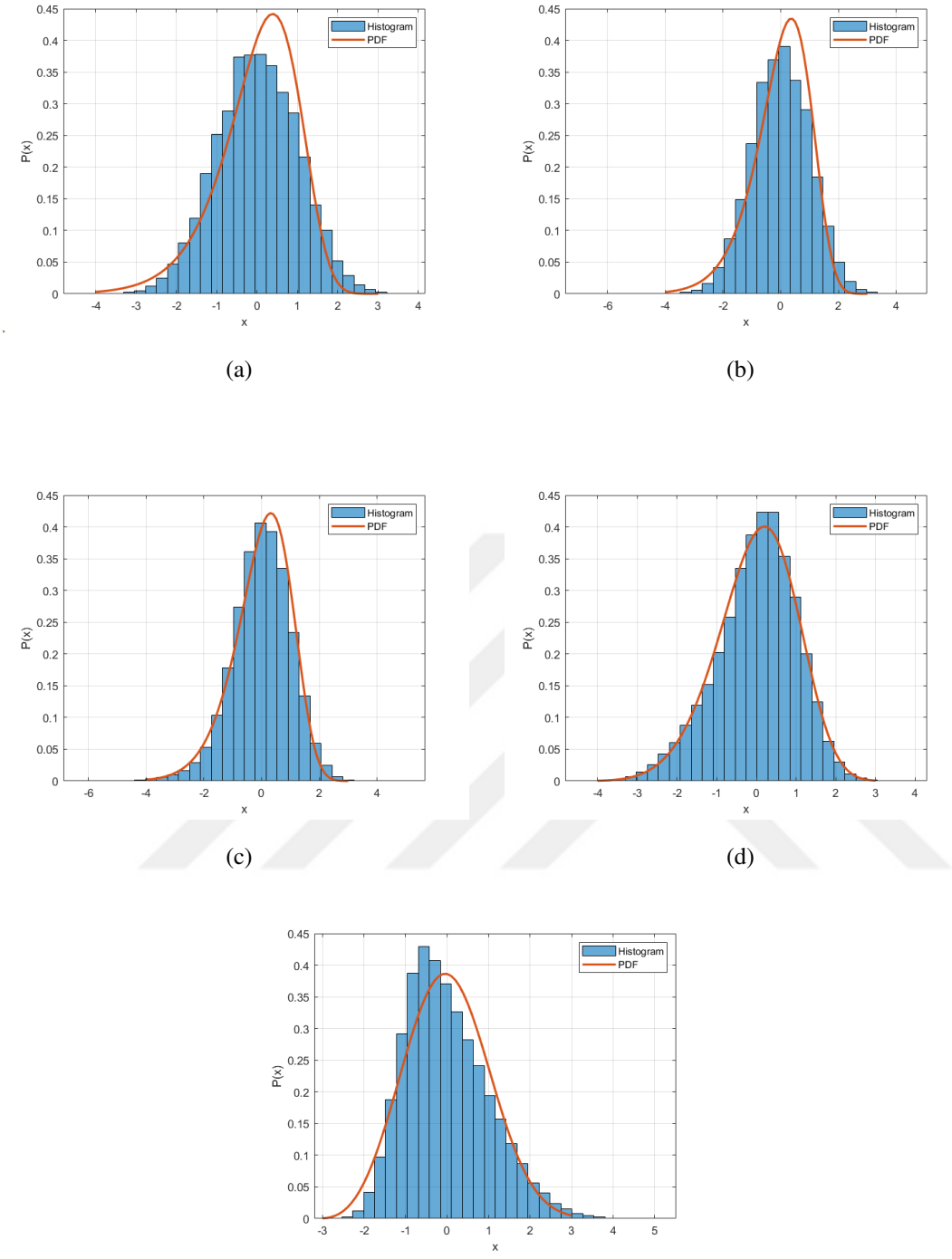
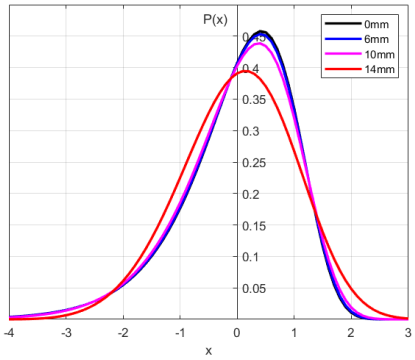
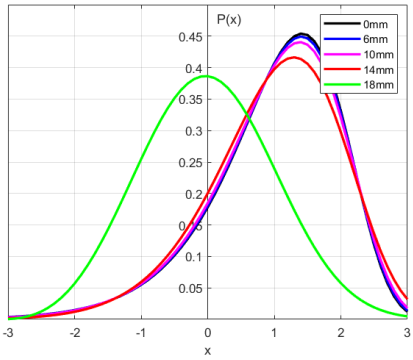


Figure 4.16: PDFs and Histograms for 1D Location at 0mm(a), 6mm(b), 10mm(c), 14mm(d), 18mm(e).

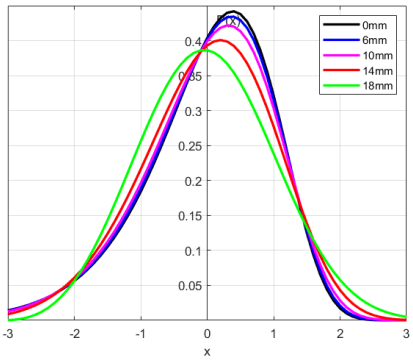
Also, PDFs of different traverse positions for each different measurement location are plotted together as in the below figures.



(a)



(b)



(c)

Figure 4.17: PDFs for 0.3D location(a), 0.5D location(b), 1D location(c)

From the figure 4.17 that shows PDFs for 0.3D location, it can be observed that while PDFs for 0 mm, 6 mm and 10 mm are similar to each other, the PDF for 14 mm is more symmetrical. Also, in the figure **??** that depicts PDFs for 0.5D location, the PDF for the 18 mm is significantly different from others. The PDFs for 0 mm, 6 mm, 10 mm and 14 mm are much more skewed when compared to those for other locations as well. At 1 diameter away from the exit of the jet, as figure **??** depicts, PDFs become more similar while the ones for 14 mm and 18 mm are still more symmetrical than the rest. Therefore, it can be concluded that when the flow is more developed, PDFs

become more symmetrical.

4.3.2.1 Spectral Study

As another important part of the analysis, spectra based on frequency are obtained for each point and for each location as follows.

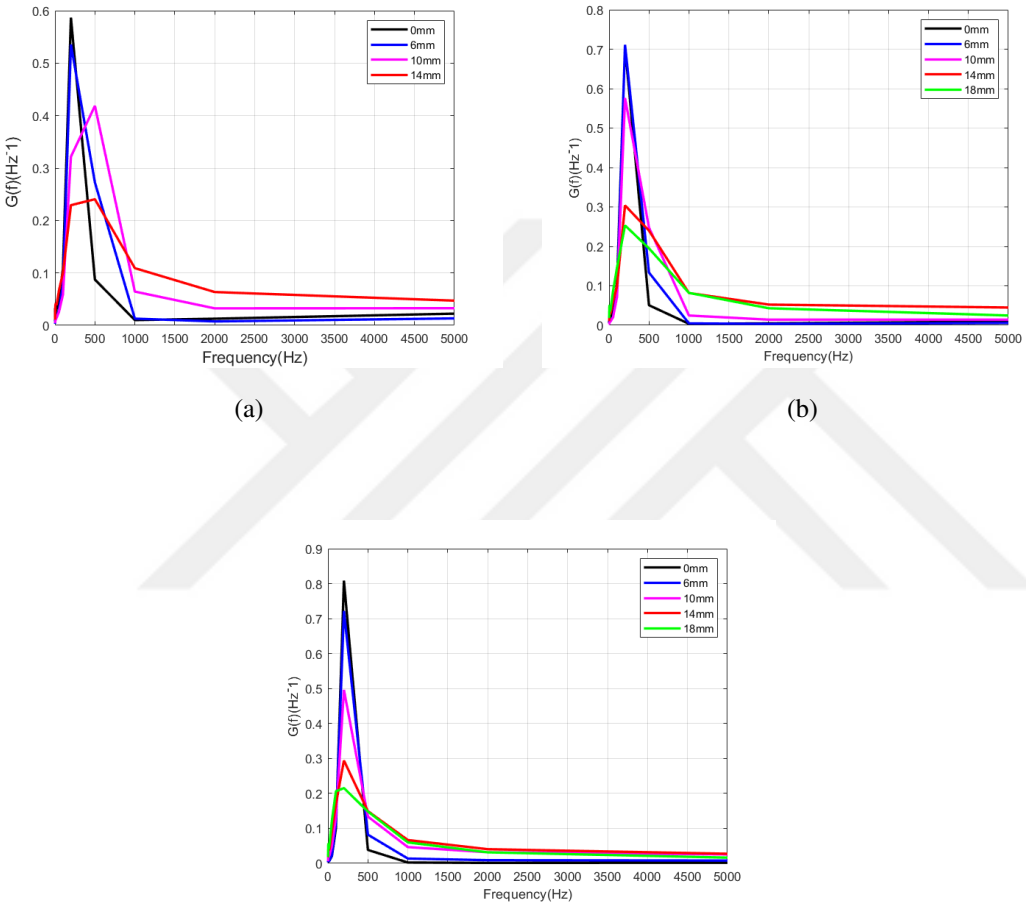
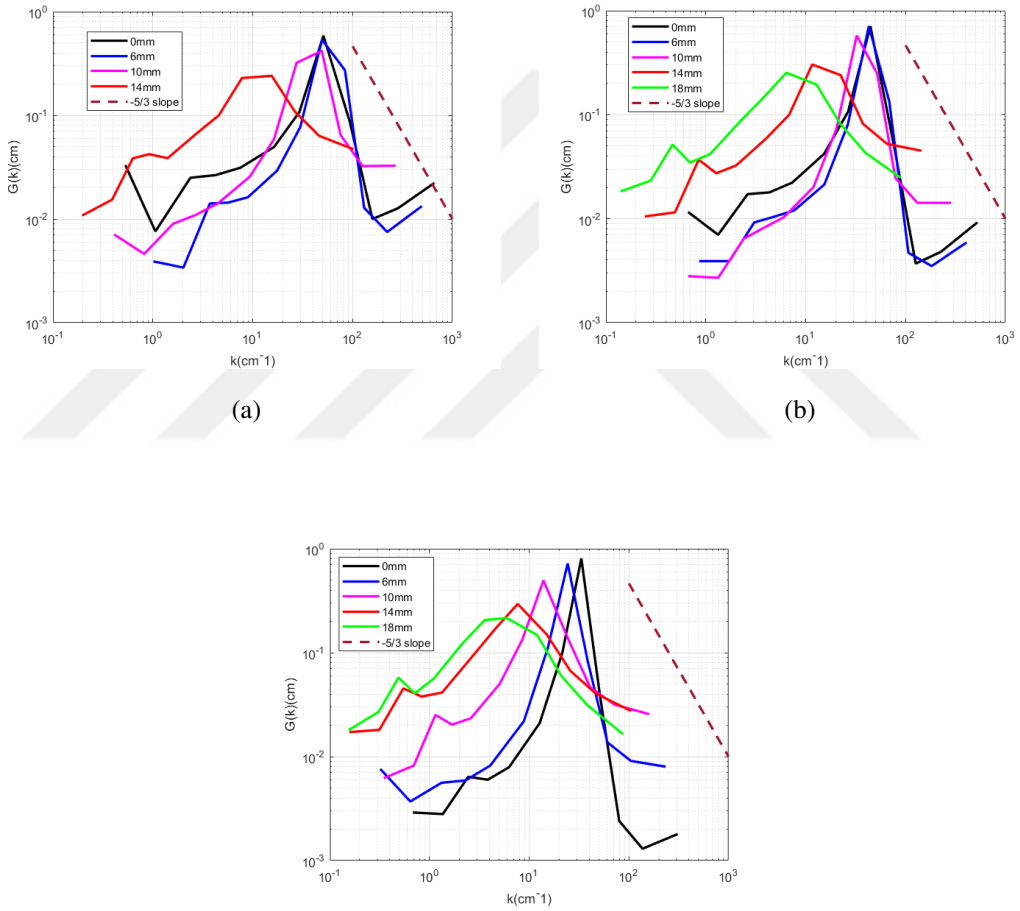


Figure 4.18: Spectra based on frequency for 0.3D location(a), 0.5D location(b), 1D location(C)

Firstly, it is obvious that energy densities contained in 0-500 Hz frequency interval decreases as the traverse position increases for each location. Also, the energy densities contained in the 100-5000 Hz interval, is mostly decreasing with decreasing traverse

position. It means, the fluctuations that occur at higher frequencies like 1000 Hz and above contains more energy for outer regions rather than the jet center while the situation is the inverse for fluctuations with lower frequencies. Also, when the distance from the jet exit is increased in the direction of the flow, energy densities contained in 0-500 Hz range increase near the jet center. However, for 10 mm, 14 mm, and 18 mm locations there is a slight decrease in energy densities when we move from 0.5D location to the 1D location.

Also, spectra based on wave number on a logarithmic scale are obtained for each point, and for each location they are plotted separately as follows.



(a) (b)

(c)

Figure 4.19: Spectra based on wavenumber for 0.3D location(a), 0.5Dlocation(b), 1D location(c)

It can be observed from the above figures that, when traverse location increases, that

is, we move away from the axis of the jet, spectra starts from smaller wavenumbers, and therefore, larger eddies are formed. This is a reasonable result as in the outer regions, the jet flow starts to interact with the ambient air. Also, in outer traverse locations, the eddies of the same size as the ones for the other traverse locations closer to the jet axis are more energetic. It can also be seen that for 14 mm and 18 mm traverse locations, slopes of the inertial subrange of the spectra are more close to -5/3 than the other traverse locations.

In addition, the largest eddie sizes, turbulence intensity, and mean velocity for each traverse position and for each location are tabulated as follows.

It can be observed from the tables that eddies become larger when we move away from the jet axis. It is expected since larger velocity gradients are formed because of the interaction of ambient air and jet.

Traverse Position(mm)	Largest Wavelength(cm)	Turbulence Intensity(-)	Mean Velocity(m/s)
0	1.8845	0.0266	10.0658
6	0.9872	0.0364	10.1299
10	2.4401	0.0690	9.9084
14	5.1029	0.2198	7.6179

Table 4.2: Some characteristics of the flow at 0.3D location

Traverse Position(mm)	Largest Wavelength(cm)	Turbulence Intensity(-)	Mean Velocity(m/s)
0	1.5065	0.0349	10.1557
6	1.1641	0.0448	10.1830
10	1.5013	0.0648	9.9806
14	4.0742	0.1299	9.1908
18	7.1257	0.3093	5.9935

Table 4.3: Some characteristics of the flow at 0.5D location

Traverse Position(mm)	Largest Wavelength(cm)	Turbulence Intensity(-)	Mean Velocity(m/s)
0	1.4685	0.0615	10.1714
6	3.1121	0.0790	10.1000
10	2.8744	0.1131	9.6339
14	6.3640	0.1881	8.3039
18	6.4588	0.3139	5.8854

Table 4.4: Some characteristics of the flow at 1D location

CHAPTER 5

CONCLUSIONS

Turbulent flows are encountered in various engineering applications. However, the problems of turbulence can be quite intricate. Undoubtedly, one of the most challenging problems of turbulence is representing all regions in the spectrum mathematically. Taylor's Frozen Turbulence approach and its mathematical implications give realistic results for the universal equilibrium region but it fails to represent the large eddies region. Also, the validity of this approach relies on some necessary conditions such that the flow must be uniform, turbulence intensity must be low, etc. Therefore, representing turbulence for other cases such as shear flow or compressible flow becomes a question that needs to be solved. In addition to that, new methods are required to represent the regions with large eddies mathematically. To overcome those difficulties, engineers used models such as LES, however, models have their own restrictions, and they are specific to the case. Another popular approach in the literature is adjusting Taylor's hypothesis by means of some corrections for the convection velocity in the dispersion relation and employing those corrections for the case under investigation. However, although they are useful in engineering applications, these approaches and methods do not aim to understand the physical mechanisms of turbulence. To represent the entire spectrum and to represent any turbulent flow no matter what the boundary conditions are, it is vital to develop a perspective totally based on the physics of turbulence. In line with this purpose, it is appropriate to consider turbulence in terms of eddies, as eddies constitute the building blocks of turbulence. As is known, large eddies are formed where the large gradients of velocity occur, such as near the boundaries. It means that, unlike the universal equilibrium region, large eddies have the information of the characteristics of the specific flow field under investigation. Since Taylor's approach suggests the mean velocity as convection ve-

locity in the dispersion relation, it treats all types of flows with all types of boundary conditions equally as long as they have the same local mean velocity. Thus, it is successful in the universal equilibrium region but fails in the large eddies region, which represents the distinctive characteristics of the specific case. In addition, when the spectrum is considered, large eddies contain a significant amount of energy that cannot be ignored. In the light of these, Çıray(1980) proposed a new approach, namely QBT, to understand the physics of turbulence and to represent it mathematically in conformity to its physics[6]. QBT defines a dispersion relation in which the convective velocity is given as the group velocity of eddies, which is also equal to the fluctuating part of the instantaneous velocity. In this way, the motion of eddies is defined both as the motion of a particle that has a translational velocity and as a motion of a wave that has a group velocity. Because of this double character, it is claimed that the turbulence has a 'quantic' behavior[8].

In this thesis study, a Matlab code is developed based on the mathematical procedure defined by Çıray(1980) and it is used to analyze different turbulent flow data. The code consists of two parts each of which has separate functions. The first part takes the instantaneous velocity data as input and by performing Fast Fourier Transform, it returns the energy density values corresponding to certain frequency ranges as output. The second part takes those energy values as input and following the mathematical procedure of QBT, produces a PDF and returns wavenumbers associated with certain frequency values by utilizing the dispersion relation suggested by Çıray. Implementation of mathematical procedure of QBT is tested and verified by utilizing the code for the various data in Çıray's study in 1980.

After verification of the code, two different experimental data are analyzed and results are presented. The first experiment that is conducted by Akpolat et al. is about the placement of an MVG inside a wind tunnel. Firstly, the data of the undisturbed boundary layer of the wind tunnel is collected by traversing a hot wire probe at a fixed distance from the inlet. As a second case, an MVG is placed inside the wind tunnel and the same procedure is repeated for the same measurement location. After obtaining the velocity profiles of these two cases, 4 points are chosen to be analyzed. For each of those points, energy contents of twelve frequency intervals are obtained and energy spectra based on frequency are plotted. Based on the spectra, the effect of

MVG is observed as in the presence of MVG, the flow becomes more energetic. Also, it is observed that for the undisturbed case, that is without MVG, energy densities are decreased with the increasing distance from the walls. However, for the MVG case such a relation cannot be inferred as it mixes the upper and lower regions of the boundary layer. Using the second part of the code, PDFs are obtained for each point and for both cases. In order to find out whether PDFs represent the data accurately, histograms are also plotted. It is observed that the PDFs are fitted to the histograms well, in general. In addition, spectra based on wavenumber are obtained for both cases and at each point. It is observed that in the energetic eddies and universal equilibrium regions, the MVG case has higher energy density values than the undisturbed case, whereas in the large eddies region this situation is reversed. Also, $-5/3$ slope is observed for the inertial subrange of the spectrum, which is in line with the literature. One of the most significant results is that the largest eddie sizes are in conformity with the physical domain of the experiment. For this experiment, boundary layer thicknesses for each case can be thought of as the intrinsic dimensions of the physical domain and results show that the largest eddie sizes are smaller than the boundary thicknesses for each case.

In the second part, unconfined and non-swirling jet data is analyzed by using the same procedure as in the MVG experiment. It is observed that the jet flow has different characteristics than the boundary layer. The data is collected at three different locations downstream of the jet and as expected, flow becomes more developed as the distance increases. Also, hotwire probes are employed to take measurements along the cross-section of the jet flow. By traversing the hot wire probes by 1mm increments data is obtained for 34 different points. However, analysis is carried out up to 18 mm due to the aforementioned reasons. Again, it is observed that the PDFs suggested by QBT conform to the histograms obtained by using the experimental data in general. Also, carrying out a spectral analysis, it is observed that larger eddies are formed when we move away from the jet center and also move farther in the direction of the flow. Thus, it is inferred that the spectra represent the physical phenomena accurately.

REFERENCES

[1] Abramowitz, M., *Handbook of Mathematical Functions, edited by M. Abramowitz and I. Stegun*, Dover Publications, New York, 1964.

[2] Akpolat, M., T., Abdulrahim, A., Hassanein, A., Uzol, O. and Perçin, M., Experimental Characterization of Micro Vortex Generators in Low Speed Flows, *Ankara International Aerospace Conference*, 2021.

[3] del Alamo, J.C., Jimenez,J., Estimation of turbulent convection velocities and corrections to Taylor's approximation, *Journal of Fluid Mechanics* , 640,pp.5-26, 2009.

[4] Moin,P., Revisiting Taylor's hypothesis, *Journal of Fluid Mechanics* , 640,pp.1-4, 2009.

[5] Ciray, C., Türbülansın bir problemi ve 'Türbülansın quantik davranışı' yaklaşımıyla çözümü, *UHUK*, 2020.

[6] Çıray, C., On wave number definition in turbulence, *METU Journal of Pure and Applied Sciences Vol 13, No 3, pp: 431-480*, 1980.

[7] Çıray, C., *Akışkanlar Mekaniğine Giriş Üçüncü Kitap*, Odtü Yayıncılık, 2013.

[8] Çıray, C., Quantic behavior of turbulence, *In 10th Ankara International Aerospace Conference.*, METU, Sep., 2019.

[9] Çıray, C., Wavenumber in turbulence and its discrete nature, *In 9th Ankara International Aerospace Conference*, METU, Sep., 2017.

[10] Fisher,J.J., Davies P.O.A.L , Correlation Measurements in a nonfrozen pattern of turbulence (broadband and wavenumber dependent) in a plane jet, *Journal of Fluid Mechanics*, 18 pp.99-116, 1964.

[11] Geng,C., He,G., Wang Y., Xu,C., Lozano-Duran, A., Wallace, J.M., Taylor's

hypothesis in turbulent channel flow considered using a transport equation analysis, *Physics of Fluids*, 27, 025111, 2015.

[12] G. I. Taylor., The spectrum of turbulence, *Proceedings of the Royal Society of London. Series A-Mathematical and Physical Sciences*, 164(919):476–490, 1938.

[13] Goldschmidt, V.W., Young, M.F., Ott, E.S. Turbulent convective velocities(broadband and wavenumber dependent) in a plane jet, *Journal of Fluid Mechanics*, 105 pp.327-345, 1981.

[14] Hinze, J.O., *Turbulence: An Introduction to Its Mechanism and Theory*, McGraw-Hill, 1975.

[15] de Kat, R., Ganapathisubramani, B., Frequency-wavenumber mapping in turbulent shear flow, *Journal of Fluid Mechanics*, 783,pp.166-190, 2015.

[16] Kıyıcı, F. and Perçin, M., Experimental Investigation of the Confinement Effects in Radial-Radial Swirlers, *Proceedings of ASME Turbo Expo 2021 Turbomachinery Technical Conference and Exposition* GT2021 June 7-11, 2021.

[17] Landau, L.D., Lifshitz E.M., *Fluid Mechanics*, Pergamon Press, 1959.

[18] Lee, S., Lele, S.K., Moin, P., Simulation of spatially evolving turbulence and the applicability of Taylor's hypothesis in compressible flow, *Physics of Fluids A: Fluid Dynamics* , 4, 1521, 1992.

[19] Reynolds, O., On the dynamical theory of incompressible viscous fluids and the determination of the criterion, *Philosophical transactions of the royal society of London* , (a.), (186):123–164, 1895.

[20] Sun, Z. Micro Vortex Generators for Boundary Layer Control: Principles and Applications, *International Journal of Flow Control*, 7(1-2), 67-86, 2015.

[21] Tardu, S., Vezin, P., On the Taylor hypothesis in forced unsteady wall flows *Experiments in Fluids*, 39,pp.909–922, 2005.

APPENDIX

TABLES FOR THE MVG EXPERIMENT

Table .1: Results of Undisturbed case at 14mm

$\overline{U}$ =7.7533 m/s I_{act}=0.0091 n=11.5841 B=0.2207
u'=10.7683 m/s I_{calc}=0.0091 $P(0)$=4.001 A=0.9675

f	ΔG	x	k	L	$P_R(x)$	$P_L(x)$
Hz	-	-	cm^{-1}	cm	-	-
0		-	-	-	0.4001	0.4001
	0.0307					
1		0.4864	0.2157	4.6354	0.4210	0.3039
	0.0163					
2		0.5668	0.4315	2.3177	0.4126	0.2857
	0.0361					
5		0.6947	0.8643	1.1570	0.3917	0.2570
	0.0424					
10		0.8076	1.4529	0.6883	0.3657	0.2323
	0.0577					
20		0.9308	2.4655	0.4056	0.3306	0.2065
	0.0802					
50		1.0620	5.1014	0.1960	0.2870	0.1808
	0.0476					
100		1.1424	8.9517	0.1117	0.2583	0.1661
	0.0401					
200		1.2082	16.1103	0.0621	0.2343	0.1546
	0.0362					
500		1.2668	36.4169	0.0275	0.2128	0.1449
	0.0151					
1000		1.2921	68.6940	0.0146	0.2036	0.1408
	0.0056					
2000		1.3017	131.9848	0.0076	0.2001	0.1392
	0.0013					
5000		1.3040	320.4571	0.0031	0.1993	0.1389

Table .2: Results of Undisturbed case at 34mm

$\overline{U}$ =8.7846 m/s I_{act}=0.0731 n=16.1690 B=0.1872

u'=0.6418 m/s I_{calc}=0.0731 $P(0)$=0.4026 A=0.9735

f	ΔG	x	k	L	$P_R(x)$	$P_L(x)$
Hz	-	-	cm^{-1}	cm	-	-
0		-	-	-	0.4026	0.4026
	0.0186					
1		0.4107	0.2932	3.4103	0.4367	0.3165
	0.0083					
2		0.4676	0.5865	1.7051	0.4344	0.3032
	0.0240					
5		0.5845	1.2145	0.8234	0.4325	0.2760
	0.0404					
10		0.7183	2.0520	0.4873	0.4002	0.2455
	0.0427					
20		0.8263	3.4149	0.2928	0.3734	0.2219
	0.0743					
50		0.9738	6.9693	0.1435	0.3268	0.1917
	0.0435					
100		1.0526	11.9961	0.0834	0.2982	0.1767
	0.0328					
200		1.1099	21.2969	0.0470	0.2764	0.1662
	0.0293					
500		1.1598	47.7590	0.0209	0.2568	0.1575
	0.0111					
1000		1.1791	89.9648	0.0111	0.2492	0.1542
	0.0040					
2000		1.1862	172.9919	0.0058	0.2464	0.1530
	0.0008					
5000		1.1876	420.5916	0.0024	0.2458	0.1528

Table .3: Results of Undisturbed case at 54mm

$\overline{U}$ =9.5629 m/s I_{act}=0.0516 n=23.4394 B=0.1585
u'=0.4936 m/s I_{calc}=0.0516 $P(0)$=0.4049 A=0.9799

f	ΔG	x	k	L	$P_R(x)$	$P_L(x)$
Hz	-	-	cm^{-1}	cm	-	-
0		-	-	-	0.4049	0.4049
	0.0129					
1		0.3629	0.4168	2.3990	0.4460	0.3246
	0.0048					
2		0.4051	0.8337	1.1995	0.4463	0.3144
	0.0140					
5		0.4956	1.7765	0.5629	0.4433	0.2926
	0.0222					
10		0.5960	3.0606	0.3267	0.4334	0.2401
	0.0384					
20		0.7201	5.1963	0.1924	0.4113	0.2401
	0.0603					
50		0.8632	10.4993	0.0952	0.3730	0.2091
	0.0380					
100		0.9411	17.8726	0.0560	0.3469	0.1932
	0.0267					
200		0.9927	31.3989	0.0318	0.3280	0.1832
	0.0230					
500		1.0355	69.8678	0.0143	0.3114	0.1751
	0.0083					
1000		1.0510	131.3328	0.0076	0.3052	0.1723
	0.0028					
2000		1.0563	252.4460	0.0040	0.3031	0.1713
	0.0006					
5000		1.0574	613.9743	0.0016	0.3027	0.1711

Table .4: Results of Undisturbed case at 74mm

$\overline{U}$ =10.1677 m/s I_{act}=0.0311 n=39.8383 B=0.1310

u'=0.3160 m/s I_{calc}=0.0311 $P(0)$=0.4071 A=0.9871

f	ΔG	x	k	L	$P_R(x)$	$P_L(x)$
Hz	-	-	cm^{-1}	cm	-	-
0		-	-	-	0.4071	0.4071
	0.0103					
1		0.3361	0.6808	1.4688	0.4536	0.3285
	0.0031					
2		0.3680	1.3617	0.7344	0.4550	0.3205
	0.0088					
5		0.4378	2.9827	0.3353	0.4558	0.3031
	0.0144					
10		0.5202	5.2533	0.1904	0.4524	0.2827
	0.0208					
20		0.6082	9.0758	0.1102	0.4432	0.2615
	0.0371					
50		0.7246	18.8839	0.0530	0.4218	0.2345
	0.0258					
100		0.7917	32.6041	0.0307	0.4047	0.2196
	0.0188					
200		0.8364	57.7187	0.0173	0.3916	0.2100
	0.0151					
500		0.8704	129.0345	0.0077	0.3806	0.2029
	0.0051					
1000		0.8818	243.2520	0.0041	0.3768	0.2006
	0.0017					
2000		0.8855	468.7520	0.0021	0.3755	0.1998
	0.0005					
5000		0.8866	1142.3761	0.0008	0.3751	0.1996

Table .5: Results of MVG case at 14mm

$\overline{U}$ =7.9501 m/s I_{act}=0.0975 n=11.7895 B=0.1492

u'=0.7754 m/s I_{calc}=0.0975 $P(0)$=0.4003 A=0.9678

f	ΔG	x	k	L	$P_R(x)$	$P_L(x)$
Hz	-	-	cm^{-1}	cm	-	-
0		-	-	-	0.4003	0.4003
	0.0185					
1		0.4108	0.2319	4.3131	0.4262	0.2316
	0.0063					
2		0.4556	0.4637	2.1566	0.4239	0.3106
	0.0152					
5		0.5387	0.9973	1.0027	0.4167	0.2918
	0.0173					
10		0.6117	1.7494	0.5716	0.4071	0.2752
	0.0247					
20		1.6951	3.0740	0.3253	0.3924	0.2565
	0.0507					
50		0.8264	6.5711	0.1522	0.3615	0.2279
	0.0631					
100		0.9560	11.4735	0.0872	0.3232	0.2011
	0.0700					
200		1.0788	19.9495	0.0501	0.2815	0.1773
	0.0723					
500		1.1941	42.4829	0.0235	0.2397	0.1567
	0.0355					
1000		1.2518	76.4139	0.0131	0.2184	0.1470
	0.0165					
2000		1.2795	141.1454	0.0071	0.2083	0.1425
	0.0053					
5000		1.2886	331.1435	0.0030	0.2049	0.1410

Table .6: Results of MVG case at 34mm

$\overline{U}$ =7.1431 m/s I_{act}=0.1404 n=7.8191 B=0.1815

u'=1.0029 m/s I_{calc}=0.1404 $P(0)$=0.3966 A=0.9623

f	ΔG	x	k	L	$P_R(x)$	$P_L(x)$
Hz	-	-	cm^{-1}	cm	-	-
0		-	-	-	0.3966	0.3966
	0.0122					
1		0.3587	0.2134	4.6859	0.4117	0.3386
	0.0053					
2		0.4068	0.4268	2.3429	0.4093	0.3290
	0.0114					
5		0.4843	0.8889	1.1250	0.4031	0.3129
	0.0191					
10		0.5780	1.5357	0.6512	0.3917	0.2928
	0.0319					
20		0.6917	2.6197	0.3817	0.3723	0.2681
	0.0802					
50		0.8864	5.3369	0.1874	0.3263	0.2264
	0.0965					
100		1.0610	8.8709	0.1127	0.2748	0.1910
	0.0955					
200		1.2101	14.7757	0.0677	0.2269	0.1632
	0.0919					
500		1.3444	30.3081	0.0330	0.1837	0.1403
	0.0404					
1000		1.4075	53.6087	0.0131	0.2184	0.1470
	0.0180					
2000		1.4371	98.1208	0.0102	0.1551	0.1257
	0.0056					
5000		1.4466	228.9095	0.0044	0.1523	0.1243

Table .7: Results of MVG case at 54mm

$\overline{U}$ =6.6834 m/s I_{act}=0.1541 n=7.0237 B=0.2021

u'=1.0296 m/s I_{calc}=0.1541 $P(0)$=0.3955 A=0.9618

f	ΔG	x	k	L	$P_R(x)$	$P_L(x)$
Hz	-	-	cm^{-1}	cm	-	-
0		-	-	-	0.0.3955	0.3955
	0.0082					
1		0.3145	0.2432	4.1116	0.4085	0.3491
	0.0041					
2		0.3618	0.4864	2.0558	0.4068	0.3402
	0.0093					
5		0.4393	0.9925	1.0076	0.4017	0.3250
	0.0142					
10		0.5232	1.6870	0.5928	0.3930	0.3077
	0.0280					
20		0.6399	2.8535	0.3505	0.3756	0.2829
	0.0792					
50		0.8509	5.7145	0.1750	0.3299	0.2376
	0.1042					
100		1.0448	9.3005	0.1075	0.2755	0.1977
	0.1259					
200		1.2349	15.1412	0.0660	0.2167	0.1618
	0.0913					
500		1.3675	29.9661	0.0334	0.1759	0.1391
	0.0355					
1000		1.4232	52.2792	0.00191	0.1594	0.1302
	0.0154					
2000		1.4485	95.1582	0.0105	0.1520	0.1263
	0.0047					
5000		1.4565	221.5474	0.0045	0.1498	0.1251

Table .8: Results of MVG case at 74mm

$\overline{U}$ =10.2804 m/s I_{act}=0.0269 n=46.1664 B=0.0890

u'=0.2770 m/s I_{calc}=0.0269 $P(0)$=0.4076 A=0.9887

f	ΔG	x	k	L	$P_R(x)$	$P_L(x)$
Hz	-	-	cm^{-1}	cm	-	-
0		-	-	-	0.0.4076	0.4076
	0.0118					
1		0.3515	0.7084	1.4117	0.4562	0.3241
	0.0023					
2		0.3739	1.4167	0.7058	0.4571	0.3185
	0.0040					
5		0.4076	3.2369	0.3089	0.4579	0.3100
	0.0060					
10		0.4499	6.0196	0.1661	0.4577	0.2994
	0.0076					
20		0.4947	11.0611	0.0904	0.4562	0.2883
	0.0225					
50		0.5956	24.8167	0.0403	0.4472	0.2636
	0.0353					
100		0.7101	43.8594	0.0228	0.4274	0.2368
	0.0311					
200		0.7915	75.8008	0.0132	0.4071	0.2187
	0.0141					
500		0.8255	161.7805	0.0062	0.3971	0.2114
	0.0040					
1000		0.8350	299.1703	0.0033	0.3941	0.2094
	0.0016					
2000		0.8388	570.8240	0.0018	0.3929	0.2086
	0.0007					
5000		0.8404	1382.1134	0.0007	0.3924	0.2083

TABLES FOR UNCONFINED AND NONSWIRLING JET EXPERIMENT

Table .9: Results for 0.3D location and at 0 mm

$\overline{U}$ =10.0658 m/s I_{act}=0.0266 n=46.8093 B=0.1074
u'=0.2676 m/s I_{calc}=0.0266 $P(0)$=0.4076 A=0.9888

f	ΔG	x	k	L	$P_R(x)$	$P_L(x)$
Hz	-	-	cm^{-1}	cm	-	-
0		-	-	-	0.4076	0.4076
	0.0331					
1		0.4957	0.5306	1.8845	0.4563	0.2879
	0.0076					
2		0.5340	0.1.0613	0.9423	0.4538	0.2785
	0.0250					
5		0.6331	2.3803	0.4201	0.4421	0.2546
	0.0265					
10		0.7154	4.2346	0.2362	0.4264	0.2356
	0.0312					
20		0.7962	7.5166	0.1330	0.4059	0.2176
	0.0495					
50		0.9026	16.3638	0.0611	0.3716	0.1954
	0.1079					
100		1.0837	29.3704	0.0340	0.2980	0.1612
	0.5868					
200		1.6533	51.0369	0.0196	0.0659	0.0835
	0.0873					
500		1.8174	93.6414	0.0107	0.0308	0.0684
	0.0100					
1000		1.8465	158.2369	0.0063	0.0264	0.0660
	0.0127					
2000		1.8843	2853978	0.0035	0.0214	0.0630
	0.0223					
5000		1.9510	659.2275	0.0015	0.0143	0.0579

Table .10: Results for 0.3D location and at 6 mm

$\overline{U}$ =10.1299 m/s I_{act}=0.0364 n=33.7947 B=0.3087

u'=0.3689 m/s I_{calc}=0.0364 $P(0)$=0.4065 A=0.9851

f	ΔG	x	k	L	$P_R(x)$	$P_L(x)$
Hz	-	-	cm^{-1}	cm	-	-
0		-	-	-	0.4065	0.4065
	0.0039					
1		0.2432	1.0129	0.9872	0.4443	0.3519
	0.0034					
2		0.3013	2.0259	0.4936	0.4493	0.3377
	0.0141					
5		0.4362	3.7219	0.2687	0.4532	0.3044
	0.0144					
10		0.5191	5.6742	0.1762	0.4496	0.2840
	0.0162					
20		0.5902	8.9551	0.1117	0.4425	0.2669
	0.0294					
50		0.6898	17.6120	0.0568	0.4262	0.2435
	0.0770					
100		0.8724	29.9569	0.0334	0.3773	0.2037
	0.5355					
200		1.4832	49.4803	0.0202	0.1243	0.1037
	0.2725					
500		1.8232	83.9298	0.0119	0.0329	0.0687
	0.0128					
1000		1.8589	130.6391	0.0077	0.0274	0.0657
	0.0075					
2000		1.8813	222.2649	0.0045	0.0243	0.0639
	0.0133					
5000		1.9212	493.8640	0.0020	0.0195	0.0608

Table .11: Results for 0.3D location and at 10 mm

$\overline{U}$ =9.9084 m/s I_{act}=0.0690 n=17.1862 B=0.2476

u'=0.6841 m/s I_{calc}=0.0690 $P(0)$=0.4031 A=0.9746

f	ΔG	x	k	L	$P_R(x)$	$P_L(x)$
Hz	-	-	cm^{-1}	cm	-	-
0		-	-	-	0.4031	0.4031
	0.0071					
1		0.2978	0.4098	2.4401	0.4369	0.3420
	0.0046					
2		0.3536	0.8197	1.2200	0.4386	0.3292
	0.0090					
5		0.4300	1.5989	0.6254	0.4379	0.3113
	0.0109					
10		0.4973	2.6668	0.3750	0.4344	0.2955
	0.0142					
20		0.5656	4.5135	0.2216	0.4279	0.2795
	0.0257					
50		0.6609	9.3849	0.1066	0.4137	0.2575
	0.0587					
100		0.8169	16.3335	0.0612	0.3780	0.2229
	0.3216					
200		1.2756	27.5768	0.0363	0.2109	0.1377
	0.4185					
500		1.7120	49.1778	0.0203	0.0653	0.0819
	0.0644					
1000		1.8351	76.0015	0.0132	0.0404	0.0701
	0.0324					
2000		1.9120	126.0505	0.0079	0.0288	0.0636
	0.0327					
5000		1.9967	270.1625	0.0037	0.0191	0.0569

Table .12: Results for 0.3D location and at 14 mm

$\overline{U}$ =7.6179 m/s I_{act}=0.2198 n=4.6009 B=0.4466

u'=1.6744 m/s I_{calc}=0.2198 $P(0)$=0.3909 A=0.9695

f	ΔG	x	k	L	$P_R(x)$	$P_L(x)$
Hz	-	-	cm^{-1}	cm	-	-
0		-	-	-	0.3909	0.3909
	0.0154					
1		0.3460	0.1960	5.1029	0.3868	0.3540
	0.0154					
2		0.4716	0.3919	2.5514	0.3740	0.3330
	0.0385					
5		0.6457	0.6306	1.5857	0.3470	0.2997
	0.0411					
10		0.7725	0.9212	1.0855	0.3214	0.2735
	0.0386					
20		0.8666	1.4070	0.7107	0.2999	0.2506
	0.0661					
50		0.9985	2.7060	0.3695	0.2672	0.2256
	0.1001					
100		1.1625	4.5872	0.2181	0.2241	0.1916
	0.2291					
200		1.4515	7.8132	0.1280	0.1498	0.1370
	0.2405					
500		1.7357	15.5687	0.0642	0.0888	0.0928
	0.1091					
1000		1.8970	26.3788	0.0379	0.0621	0.0723
	0.0635					
2000		2.0093	46.1598	0.0217	0.0471	0.0601
	0.0471					
5000		2.1043	102.1862	0.0098	0.0365	0.0509

Table .13: Results for 0.5D location and at 0mm

$\overline{U}$ =10.1557 m/s I_{act}=0.0349 n=35.3688 B=0.2355

u'=0.3540 m/s I_{calc}=0.0349 $P(0)$=0.4067 A=0.9857

f	ΔG	x	k	L	$P_R(x)$	$P_L(x)$
Hz	-	-	cm^{-1}	cm	-	-
0		-	-	-	0.4067	0.4067
	0.0116					
1		0.3498	0.6638	1.5065	0.4527	0.3256
	0.0070					
2		0.4118	1.3276	0.7532	0.4541	0.3102
	0.0172					
5		0.5162	2.6207	0.3816	0.4507	0.2844
	0.0179					
10		0.5945	4.3398	0.2304	0.4429	0.2655
	0.0222					
20		0.6716	7.3255	0.1365	0.4307	0.2474
	0.0419					
50		0.7853	15.2541	0.0656	0.4045	0.2218
	0.1068					
100		0.9912	26.5545	0.0377	0.3346	0.1798
	0.7071					
200		1.6676	44.4605	0.0225	0.0651	0.0830
	0.0508					
500		1.7714	76.3910	0.0131	0.0416	0.0731
	0.0037					
1000		1.7815	126.4902	0.0079	0.0397	0.0722
	0.0048					
2000		1.7947	226.1202	0.0044	0.0372	0.0710
	0.0092					
5000		1.8200	522.8103	0.0019	0.0329	0.0688

Table .14: Results for 0.5D location and at 6 mm

$\overline{U}$ =10.1880 m/s I_{act}=0.0448 n=27.1882 B=0.3419

u'=0.4566 m/s I_{calc}=0.0448 $P(0)$=0.4056 A=0.9821

f	ΔG	x	k	L	$P_R(x)$	$P_L(x)$
Hz	-	-	cm^{-1}	cm	-	-
0		-	-	-	0.4056	0.4056
	0.0186					
1		0.2434	0.8590	1.1641	0.4415	0.3525
	0.0039					
2		0.3085	1.7181	0.5820	0.4465	0.3369
	0.0092					
5		0.4023	3.0562	0.3272	0.4494	0.3140
	0.0104					
10		0.4732	4.7662	0.2098	0.4479	0.2967
	0.0120					
20		0.5361	7.6742	0.1303	0.4437	0.2815
	0.0213					
50		0.6226	15.3752	0.0650	0.4333	0.2610
	0.0804					
100		8357	26.4264	0.0378	0.3847	0.2133
	0.7112					
200		1.5969	42.8918	0.0233	0.0885	0.0915
	0.1336					
500		1.8085	68.7433	0.0145	0.0379	0.0706
	0.0047					
1000		1.8214	106.7885	0.0094	0.0357	0.0695
	0.0035					
2000		1.8313	182.3381	0.0055	0.0340	0.0686
	0.0059					
5000		1.8479	407.7664	0.0025	0.0314	0.0672

Table .15: Results for 0.5D location and at 10 mm

$\overline{U}$ =9.9806 m/s I_{act}=0.0648 n=18.3902 B=0.3323
u'=0.6470 m/s I_{calc}=0.0648 $P(0)$=0.4035 A=0.9758

f	ΔG	x	k	L	$P_R(x)$	$P_L(x)$
Hz	-	-	cm^{-1}	cm	-	-
0		-	-	-	0.4035	0.4035
	0.0028					
1		0.2183	0.6661	1.5013	0.4330	0.3596
	0.0027					
2		0.2749	1.3322	0.7507	0.4372	0.3468
	0.0064					
5		0.3574	2.3920	0.4181	0.4404	0.3277
	0.0081					
10		0.4261	3.7505	0.2666	0.4400	0.3115
	0.0103					
20		0.4910	6.0297	0.1658	0.4370	0.2962
	0.0201					
50		0.5849	11.9636	0.0836	0.4277	0.2741
	0.0724					
100		0.7975	20.2652	0.0493	0.3854	0.2261
	0.5762					
200		1.4895	32.4423	0.0308	0.1292	0.1068
	0.2479					
500		1.8007	52.0011	0.0192	0.0454	0.0729
	0.0247					
1000		1.8591	78.9670	0127	0.0353	0.0677
	0.0142					
2000		1.8966	131.2025	0.0076	0.0298	0.0646
	0.0142					
5000		1.9358	284.8143	0.0035	0.0247	0.0614

Table .16: Results for 0.5D location and at 14 mm

$\overline{U}$ =9.1908 m/s I_{act}=0.1299 n=8.5473 B=0.3710

u'=1.1938 m/s I_{calc}=0.1299 $P(0)$=0.3974 A=0.9631

f	ΔG	x	k	L	$P_R(x)$	$P_L(x)$
Hz	-	-	cm^{-1}	cm	-	-
0		-	-	-	0.3974	0.3974
	0.0105					
1		0.3409	0.2454	4.0742	0.4159	0.3406
	0.0115					
2		0.4409	0.4909	2.0371	0.4112	0.3199
	0.0369					
5		0.6208	0.8490	1.1779	0.3900	0.2809
	0.0273					
10		0.7110	1.2729	0.7856	0.3733	0.2612
	0.0325					
20		0.7989	2.0131	0.4967	0.3535	0.2421
	0.0586					
50		0.9264	3.9895	0.2507	0.3193	0.2153
	0.0997					
100		1.0982	6.8301	0.1464	0.2659	0.1813
	0.3039					
200		1.4633	11.6227	0.0860	0.1467	0.1201
	0.2399					
500		1.7543	22.4130	0.0446	0.0717	0.0831
	0.0818					
1000		1.8946	37.4140	0.0267	0.0464	0.0688
	0.0524					
2000		2.0026	65.1945	0.0153	0.0316	0.0591
	0.0450					
5000		2.1082	144.0415	0.0069	0.0209	0.0508

Table .17: Results for 0.5D location and at 18 mm

$\overline{U}$ =5.9935 m/s I_{act}=0.3093 n=3.0014 B=0.4169

u'=1.8539 m/s I_{calc}=0.3093 $P(0)$=0.3864 A=1.0109

f	ΔG	x	k	L	$P_R(x)$	$P_L(x)$
Hz	-	-	cm^{-1}	cm	-	-
0		-	-	-	0.3864	0.3864
	0.0183					
1		0.4142	0.1403	7.1257	0.3537	0.3628
	0.0232					
2		0.5529	0.2807	3.5629	0.3318	0.3433
	0.0515					
5		0.7346	0.4646	2.1526	0.2973	0.3110
	0.0346					
10		0.8259	0.6952	1.4384	0.2781	0.2924
	0.0418					
20		0.9195	1.1056	0.9045	0.2576	0.2723
	0.0864					
50		1.0756	2.2114	0.4522	0.2227	0.2372
	0.1462					
100		1.2869	3.7868	0.2641	0.1762	0.1889
	0.2532					
200		1.5840	6.4204	0.1558	0.1177	0.1255
	0.1950					
500		1.8233	12.8393	0.0779	0.0797	0.0825
	0.0821					
1000		1.9514	22.1332	0.0452	0.0631	0.0633
	0.0431					
2000		2.0312	39.5010	0.0253	0.0541	0.0528
	0.0247					
5000		2.0830	89.5581	0.0112	0.0488	0.0466

Table .18: Results for 1D location and at 0mm

$\overline{U}$ =10.1714 m/s I_{act}=0.0615 n=19.4414 B=0.3326
u'=0.6260 m/s I_{calc}=0.0615 $P(0)$=0.4038 A=0.9768

f	ΔG	x	k	L	$P_R(x)$	$P_L(x)$
Hz	-	-	cm^{-1}	cm	-	-
0		-	-	-	0.4038	0.4038
	0.0029					
1		0.2209	0.6810	1.4685	0.4342	0.3588
	0.0028					
2		0.2781	1.3620	0.7342	0.4385	0.3458
	0.0064					
5		0.3592	2.4446	0.8234	0.4417	0.3268
	0.0060					
10		0.4117	3.8416	0.2603	0.4418	0.3144
	0.0079					
20		0.4657	6.2796	0.1592	0.4400	0.3016
	0.0210					
50		0.5706	12.7449	0.0785	0.4312	0.2767
	0.1003					
100		0.8497	21.5406	0.0464	0.3723	0.2142
	0.8087					
200		1.6716	33.3528	0.0300	0.0729	0.0853
	0.0384					
500		1.7482	51.3663	0.0195	0.0549	0.0776
	0.0024					
1000		1.7541	80.0732	0.0125	0.0536	0.0770
	0.0013					
2000		1.7573	137.2949	0.0073	0.0529	0.0767
	0.0018					
5000		1.7617	308.6459	0.0032	0.0520	0.0763

Table .19: Results for 1D location and at 6mm

$\overline{U}$ =10.1000 m/s I_{act}=0.0790 n=14.8450 B=0.1968

u'=0.7984 m/s I_{calc}=0.0790 $P(0)$=0.4021 A=0.9719

f	ΔG	x	k	L	$P_R(x)$	$P_L(x)$
Hz	-	-	cm^{-1}	cm	-	-
0		-	-	-	0.4021	0.4021
	0.0076					
1		0.3049	0.3213	3.1121	0.4336	0.3416
	0.0037					
2		0.3495	0.6426	1.5561	0.4346	0.3315
	0.0056					
5		0.4013	1.3181	0.7586	0.4343	0.3197
	0.0059					
10		0.4448	2.2987	0.4350	0.4328	0.3096
	0.0082					
20		0.4946	4.0678	0.2458	0.4298	0.2981
	0.0219					
50		0.5951	8.8409	0.1131	0.4189	0.2748
	0.1123					
100		0.8867	15.4533	0.0647	0.3529	0.2107
	0.7219					
200		1.6334	24.3289	0.0411	0.0882	0.0914
	0.0820					
500		1.7721	38.7828	0.0258	0.0551	0.0768
	0.0137					
1000		1.8035	60.9870	0.0164	0.0490	0.0738
	0.0091					
2000		1.8255	104.6227	0.0096	0.0450	0.0718
	0.0080					
5000		1.8454	233.9548	0.0043	0.0415	0.0700

Table .20: Results for 1D location and at 10 mm

$\overline{U}$ =9.6339 m/s I_{act}=0.1131 n=9.9916 B=0.4200
u'=1.0900 m/s I_{calc}=0.1131 $P(0)$=0.3989 A=0.9651

f	ΔG	x	k	L	$P_R(x)$	$P_L(x)$
Hz	-	-	cm^{-1}	cm	-	-
0		-	-	-	0.3989	0.3989
	0.0062					
1		0.2857	0.3479	2.8744	0.4216	0.3495
	0.0082					
2		0.3822	0.6958	1.4372	0.4209	0.3294
	0.0252					
5		0.5415	1.1482	0.8709	0.4090	0.2945
	0.0203					
10		0.6253	1.6805	0.5951	0.3972	0.2759
	0.0234					
20		0.7029	2.6023	0.3843	0.3830	0.2587
	0.0501					
50		0.8318	5.0627	0.1975	0.3529	0.2307
	0.1330					
100		1.0699	8.5279	0.1173	0.2801	0.1826
	0.4961					
200		1.5937	13.9157	0.0719	0.1068	0.1002
	0.1337					
500		1.7879	24.7668	0.0404	0.0611	0.0781
	0.0465					
1000		1.8789	40.8871	0.0245	0.0449	0.0692
	0.0317					
2000		1.9495	71.5664	0.0140	0.0346	0.0629
	0.0256					
5000		2.0121	160.2742	0.0062	0.0270	0.0577

Table .21: Results for 1D location and at 14 mm

$\overline{U}$ =8.3039 m/s I_{act}=0.1881 n=5.5530 B=0.3653
u'=1.5617 m/s I_{calc}=0.1881 $P(0)$=0.3930 A=0.9637

f	ΔG	x	k	L	$P_R(x)$	$P_L(x)$
Hz	-	-	cm^{-1}	cm	-	-
0		-	-	-	0.3930	0.3930
	0.0172					
1		0.4034	0.1571	6.3640	0.3923	0.3385
	0.0181					
2		0.5196	0.3143	3.1820	0.3796	0.3164
	0.0453					
5		0.6945	0.5465	1.8297	0.3506	0.2805
	0.0378					
10		0.7993	0.8362	1.1959	0.3281	0.2583
	0.0414					
20		0.8949	1.3395	0.7465	0.3050	0.2380
	0.0919					
50		1.0628	2.6882	0.3720	0.2598	0.2031
	0.1701					
100		1.3034	4.5810	0.2183	0.1914	0.1569
	0.2941					
200		1.6392	7.6679	0.1304	0.1055	0.1032
	0.1493					
500		1.8438	15.0311	0.0665	0.0659	0.0773
	0.0667					
1000		1.9603	25.9414	0.0385	0.0484	0.0648
	0.0405					
2000		2.0428	46.4659	0.0215	0.0381	0.0569
	0.0275					
5000		2.1060	105.5497	0.0095	0.0314	0.0513

Table .22: Results for 1D location and at 18 mm

$\overline{U}$ =5.8854 m/s I_{act}=0.3139 n=2.9458 B=0.4667
u'=1.8472 m/s I_{calc}=0.3139 $P(0)$=0.3862 A=1.0141

f	ΔG	x	k	L	$P_R(x)$	$P_L(x)$
Hz	-	-	cm^{-1}	cm	-	-
0		-	-	-	0.3862	0.3862
	0.0180					
1		0.4119	0.1548	6.4588	0.3528	0.3641
	0.0270					
2		0.5693	0.3097	3.2294	0.3275	0.3421
	0.0576					
5		0.7609	0.4889	2.0454	0.2904	0.3074
	0.0406					
10		0.8615	0.7124	1.4037	0.2690	0.2866
	0.0564					
20		0.9775	1.1072	0.9031	0.2434	0.2611
	0.1230					
50		0.1753	2.1512	0.4649	0.1995	0.2157
	0.2062					
100		1.4383	3.5983	0.2779	0.1445	0.1563
	0.2153					
200		1.6940	5.9632	0.1677	0.0990	0.1048
	0.1482					
500		1.8915	11.9869	0.0834	0.0707	0.0717
	0.0599					
1000		1.9935	20.9781	0.0477	0.0585	0.0572
	0.0315					
2000		2.0559	38.0412	0.0263	0.0518	0.0492
	0.0164					
5000		2.0922	87.6762	0.0114	0.0482	0.0449